FACULDADE DE ENGENHARIA DA UNIVERSIDADE DO PORTO

U.PORTO

FEUP FACULDADE DE ENGENHARIA
UNIVERSIDADE DO PORTO

Modelling of Radiofrequency-Induced Hyperthermia within Electric Circuits Simulators

Inês Pinto Ribeiro da Costa

Mestrado em Engenharia Biomédica

Supervisor: José Machado da Silva

October 8, 2018

Modelling of Radiofrequency-Induced Hyperthermia within Electric Circuits Simulators

Inês Pinto Ribeiro da Costa

Mestrado em Engenharia Biomédica

Faculdade de Engenharia da Universidade do Porto

October 8, 2018

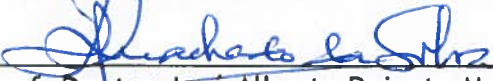**MEB – MESTRADO EM ENGENHARIA BIOMÉDICA**   **2017/2018**

A Dissertação intitulada

"Modelling of Radiofrequency-Induced Hyperthermia within Electric Circuits Simulators"

foi aprovada em provas realizadas em 21-09-2018

o júri

Presidente Prof. Doutor Joaquim Gabriel Magalhães Mendes
Professor Auxiliar do Departamento de Engenharia Mecânica da FEUP - U.Porto

Prof. Doutor José Alberto Peixoto Machado da Silva
Professor Associado do Departamento de Engenharia Eletrotécnica e de Computadores - FEUP - U. Porto

Dr. João Carlos Azevedo Gaspar
Diretor de Grupo de Investigação do INL - International Iberian Nanotechnology Laboratory

O autor declara que a presente dissertação (ou relatório de projeto) é da sua exclusiva autoria e foi escrita sem qualquer apoio externo não explicitamente autorizado. Os resultados, ideias, parágrafos, ou outros extratos tomados de ou inspirados em trabalhos de outros autores, e demais referências bibliográficas usadas, são corretamente citados.

Autor – Inês Pinto Ribeiro da Costa

Faculdade de Engenharia da Universidade do Porto

Resumo

O presente trabalho aborda o uso da radiação eletromagnética em hipertermia induzida como forma de ablação de tumores. A ablação térmica refere-se à destruição de tecidos biológicos por meio de hipertermia, isto é, através do aquecimento, a temperaturas a que as células não sobrevivem. O conceito de hipertermia no tratamento de tumores surgiu baseado em observações de que as células cancerígenas exibem maior sensibilidade ao calor do que as células normais. A hipertermia local pode ser realizada por convecção/condução ou através de radiação eletromagnética. No que diz respeito à radiação eletromagnética, podem ser considerados três grupos distintos, de acordo com o intervalo de frequências, ultrassons, radiofrequências e micro-ondas. A modelação e simulação do aquecimento dos tecidos tem sido alvo de inúmeras pesquisas. A maior parte desses estudos recorre a simulações computacionais baseadas em métodos numéricos avançados, como o método dos elementos finitos (FEM) e o método das diferenças finitas no domínio do tempo (FDTD). Atualmente, estão disponíveis várias ferramentas de simulação, como o COMSOL Multiphysics, Ansys e Sim4Life, que permitem a construção de modelos, a sua resolução por métodos numéricos, simulação e pós-processamento de resultados. Apesar de estas serem ferramentas eficientes e precisas, não permitem a realização de simulações num ambiente único, que também incluam circuitos eletrónicos de sistemas de geração de radiação eletromagnética. Nesse sentido, o presente trabalho visa trazer a propagação eletromagnética bem como o aquecimento dos tecidos para o domínio da simulação elétrica, para assim obter um ambiente de simulação de todo o processo. Isto envolve a modelação do caminho de propagação da radiação, desde o emissor de radiação, através do ar, até ao tecido alvo, bem como, do processo térmico – isto é, aquecimento local e condução da potência dissipada – tudo com modelos elétricos. O ambiente de simulação considerado é o Advanced Design System (ADS).

ii

Abstract

The present work addresses the use of electromagnetic radiation in induced hyperthermia as a treatment for cancer diseases. Thermal ablation refers to the destruction of a biological tissue by means of hyperthermia, i.e., through heating, at temperatures at which cells do not survive. The concept of hyperthermia for treating tumors has been explored after observations that cancer calls exhibit greater sensitivity to heat than normal cells. Local hyperthermia can be performed by convection/conduction or by electromagnetic radiation. Concerning electromagnetic radiation three distinct groups of frequency bandwidths can be considered, ultrasounds, radiofrequencies and microwaves. Modelling and simulation of tissue heating subject of different research activity. Most of these studies resort to computational simulations based on advanced numerical methods, such as the finite element method (FEM) and finite difference time-domain (FDTD). Several simulation tools are currently available that allow the construction of models, their resolution by numerical methods, simulation and postprocessing of results, such as COMSOL Multiphysics, Sim4Life and Ansys. Although these tools are efficient and accurate, they do not allow the realization in a single environment of simulation that also include the electronic circuits of the systems generating the electromagnetic radiation. The present work aims at bringing the electromagnetic propagation and the heating of the tissues to the domain of the electrical simulation, and thus to obtain a unique simulation environment for the entire process. This involves modelling the radiation propagation path, from the radiation emitter, through the air, until the target tumor tissue, as well as, the thermal process – i.e., local heating and conduction of the dissipated power – all with electrical models. The advanced Design System (ADS) simulation environment is being considered.

Acknowledgments

First, I want to start by thanking my supervisor José Machado da Silva who supported me in all the doubts I had during my dissertation.

I would also like to thank the great institution of FEUP and its faculty, who were able to prepare me for a demanding world in a unique way.

I express gratitude to my parents and my brothers who supported me and helped me to reach this level, for the conditions provided and for their support and patience in all the difficult times.

Finally, to my friends who, directly or indirectly, were always present in all the stages of this journey with friendship and fun.

Inês Pinto Ribeiro da Costa

*"Whether you think you can
or whether you think you can't
you're right"*

Henry Ford

Contents

List of Figures

List of Tables

Abbreviations and Symbols

List of abbreviations (sort by alphabetical order)

ADS	Advanced Design System
CAD	Computer-Aided Design
DC	Direct Current
EM	Electromagnetic
FDTD	Finite Difference Time Domain
FEM	Finite Element Method
FEUP	Faculdade de Engenharia da Universidade do Porto
HIFU	High-Intensity Focused Ultrasound
MEMS	Microelectromechanical systems
MW	Microwave
RF	Radio-frequency
SAR	Specific Absorption Rate

List of symbols

v	Velocity of propagation
f	Frequency
λ	Wavelength
γ	Propagation constant
ω	Angular frequency
α	Attenuation constant
β	Phase constant
δ	Penetration depth
μ	Magnetic permeability
E	Electric field intensity
$\tan \delta$	Loss tangent
σ	Electric conductivity
ρ	Density
ε	Permittivity
ε'	Relative permittivity
ε_0	Vacuum permittivity
k	Thermal conductivity
R_{el}	Electric Resistance
C_{th}	Thermal capacity
R_{th}	Thermal resistance
R_{heat}	Heat resistance
Q	Power density

Chapter 1

Introduction

Hyperthermia, also called thermal therapy or thermotherapy, is a type of treatment in which biological tissues are exposed to high temperatures. Several researches have shown that high temperatures can damaged and kill cancerous cells, generally without damaging or causing only minimal lesions in the normal tissue. In other words, hyperthermia or ablation at high temperatures, including the use of high-intensity focused ultrasounds, radio-frequencies and microwaves, emerged as an alternative to the standard surgical therapies. Each therapy works differently but all converge to the same purpose, which consists in heating the tissues up to 40 to destroy cancer cells within a target section of the tumor [17, 18].

Hyperthermia methods involve the transfer of heat from an external energy source to a body. Local or regional hyperthermia, systemic or hole body hyperthermia are examples of heating methods. Local hyperthermia is used to heat a target area of the body, being a process that resorts to elevated temperatures to destroy the heated cells. In local hyperthermia, the heating process can be performed by convection, conduction or through electromagnetic radiation. The most recurrent practices of local hyperthermia are those based on electromagnetic (EM) radiation due to its ability of penetrating tissues in depth. However, other techniques such as contact or deep heating or body immersion in warm water have been also used. The whole-body treatment is more often performed in generalized diseases situations, such as a metastatic tumor spread over the organism. This treatment can be made by several techniques like steam heating, warm water, electromagnetic radiation, infrared radiation, or through thermal chambers or warm water blankets [18, 8].

Regarding the application of radiation in hyperthermia ablation techniques, three distinct groups of frequency bandwidths can be considered, ultrasound, radio-frequencies and microwaves. High-intensity focused ultrasound ablation (HIFU) is an extra-corporeal technique that typically uses frequencies in the range of 0.8-1.6 MHz. This approach consists in the ultrasound waves travelling through tissues to a target region, where the sound energy is absorbed as heat. In its turn, radiofrequency ablation generally uses frequencies under 900 kHz. Most of the devices works in the 375-500 kHz frequency bandwidth. In this technique the alternating high frequency current travels through tissues, that forces the molecules movement in one direction and then, in the opposite direction. Thus, the changes in the molecule energy state results in a local temperature in-

crease due to friction. Finally, the microwave ablation technique refers to methods that comprises frequencies above 900 kHz. In the tissues, heating occurs because the electromagnetic field forces the oscillation of water molecules within cells, leading to its fast agitation and, consequently, the production of heat [19, 17].

Hyperthermia ablation is a particular case of heat transfer where, beyond the natural mechanisms of convection and conduction, also the energy coming from an external heat source interferes in the generation, storage and absorption of heat. Thus, hyperthermia constitutes a transient state heat transfer problem, i.e., a problem in which the temperatures field varies with time, being described by the Penne's bioheat equation, that allows obtaining the tissue's resulting temperature after its exposure to electromagnetic radiation [20, 21].

The human body exposure to electromagnetic fields has been the subject of several investigations that have shown reliable results of the effects to that exposure in human models through numerical methods and simulations. Most of heat transfer problems are situations that involve complex geometries, are non-linear problems and its initial and boundary conditions lead to the need of solving complex numerical methods. Finite element methods (FEM) and finite difference time-domain (FDTD) are the recurrent numerical methods to solve this kind of problems. These approaches are the most used in the available simulation tools for model's construction, resolution by the referred numerical methods, simulation and results post-processing, such as COMSOL Multiphysics [22], Ansys [23] and Sim4Life [24]. Although these are efficient and accurate tools that provide means to calculate electromagnetic fields and temperatures in a three-dimensional domain, they do not allow the realization of simulations in a unique environment that also includes the electronic circuits of the electromagnetic radiation generating systems [25, 26].

In this sense, to bring the electromagnetic propagation and the tissues heating to the electrical simulation domain to obtain a unique simulation environment of the entire process, an electrical equivalent model was developed that allows the simulation of the propagation and of the effects of electromagnetic radiation on biological tissues. The model consists in an electrical circuit where, the power supply represents the radiofrequency emission source, the transmission lines represents the propagation of radiation and each tissue layers, skin, adipose tissue, breast gland and tumor are represented by a RC electrical equivalent circuit. With this model not only becomes possible to perform a study of temperature variation in a tissue with time, but it is also allowed to simulate the electromagnetic propagation through air and tissues, as well as the operation of the electronic circuits that generate the EM field.

However, the model only allows the two-dimensional perception of the process and as it is known, the electromagnetic radiation does not propagate only in one direction but in many directions, through the entire volume of tissue. In this sense, the need of building a three-dimensional model provides a more accurate approach for the simulation. This model consists of a grid of several nodes represented by an RC equivalent circuit in which, each node represents an elementary volume of tissue. With this model, in first place, it is intended to validate the propagation of electromagnetic radiation on the different directions, through a volume of tissue. Once this validation is performed, it is intended to study the power dissipation and variation of temperature

in the different tissue layers of the three-dimensional model.

This document is organized in six chapters, including this one. In chapter 2, it is presented a theoretical background about electromagnetic radiation and its biological effects and the hyperthermia ablation is explored with the aim of understanding what it is and how it is used for therapeutic applications. Chapter 3 addresses some background about the thermal equilibrium of the human body, including a description of the Penne's bioheat equation with the aim of understanding what variables are involved in this phenomenon, how it is applied, and why it is important to simulate the heating of tissues. Furthermore, it is presented a description of currently available simulation methods and some examples of simulation software. Chapter 4 is dedicated to the presentation of the model developed in which, in first place, it is presented a review of electrical circuits and an explanation of the analogy with thermal circuits (variables, equations, etc.). In addition, it is presented a theoretical context about the dielectric behavior of cells and of their RC electrical circuit equivalent, as well as a description of the equivalent model developed. In chapter 5 is dedicated to present the results of the simulations carried out in the ADS software for the validation of the model as well as the simulations performed with the three-dimensional model. The last chapter, chapter 6, addresses the discussion of the simulation results, the conclusion of the work and some perspectives for future work than can be made to improve the obtained results.

Chapter 2

Thermal Ablation of Tissues after Hyperthermia with Electromagnetic Radiation

2.1 Electromagnetic Radiation

2.1.1 Electromagnetic Waves and Electromagnetic Fields

Electromagnetic (EM) radiation regards to the EM waves field that propagates "indefinitely" through space. EM waves cover the entire spectrum where, radio-frequencies, microwaves, visible light, etc., are examples of EM radiation. The EM waves can be defined according to its amplitude, wavelength (λ), frequency (f) and velocity (υ). The amplitude regards to the wave intensity, the wavelength is the distance between two identical points in adjacent cycles and, the wave frequency represents the number of complete wave oscillations per unit time. The wave velocity is equal to the product between frequency and wavelength, and its magnitude depends on the nature of the material through which the wave propagates and on the radiation frequency. The maximum EM wave velocity ($3x10^8$ *m/s*) occurs in vacuum and, in matter, such as tissues, the velocity depends on the characteristics of the medium. The EM waves propagates at a constant velocity in a specific medium and consequently, its frequency and wavelength are inversely proportional, equation 2.1. Figure 2.1 illustrates the EM spectrum, where it is possible to observe different examples of application according to its frequency (or wavelength) [27, 28].

$$\upsilon \;=\; \frac{\lambda}{f} \tag{2.1}$$

An EM field is a characteristic of space caused by the movement of charged particles. All charged particles, in the steady-state, produce an electric field. Otherwise, charged particles in motion generate a magnetic field. The mutual interaction between the electric and magnetic fields produces the EM field. The EM field is characterized by four main vector field quantities: electric
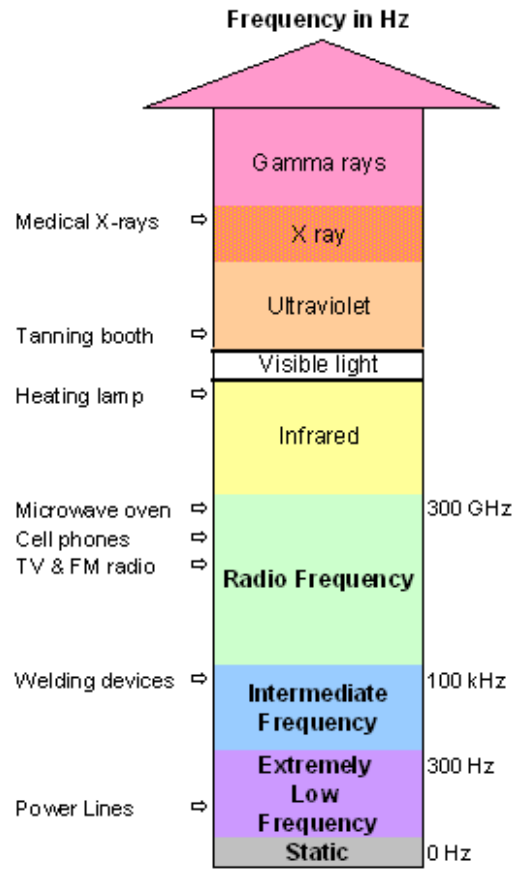
Figure 2.1: Spectrum of Electromagnetic Radiations [1].

field intensity (E), electric flux density (D), magnetic field intensity (H), and magnetic flux density (B). The electric field (in V/m) describes the force (in Newtons) per unit charge (in Coulombs). The magnetic field is defined as the magnetic force acting on a moving unit charge, with a given velocity and is expressed in ampere per meter (A/m) [28, 5, 29].

The product between the electric field and the permittivity (ε) gives the electric flux density, which regards to the measure of how much electric flux flows along a unit area and is expressed in coulombs per unit area (C/m^2), equation 2.2. Moreover, the electric field together with the electric conductivity σ is used to determine the current density (J) (in A/m^2), equation 2.3. Similarly, the magnetic flux density is determined after the product between the magnetic field and permeability (μ) and is expressed in Tesla (T) or volt-second per square meter, equation 2.4 [28, 5, 29].

$$D \;=\; \varepsilon \cdot E \qquad\qquad (2.2)$$

$$J \;=\; \sigma \cdot E \qquad\qquad (2.3)$$

$$B = \mu \cdot H \tag{2.4}$$

Electromagnetic radiation propagates as a pair of oscillatory electric and magnetic fields which are perpendicular to each other and to the direction of propagation of the wave (see figure 2.2) and, that propagates with a propagation constant γ that depends on the characteristics of the medium that it passes through. The propagation constant can be determined by the following equation:

$$\gamma = \sqrt{j\omega\mu\sigma - \omega^2\mu\varepsilon} \tag{2.5}$$

where ω is the angular frequency, μ is the magnetic permeability, ε is the electric permittivity and σ is the electric conductivity [5].
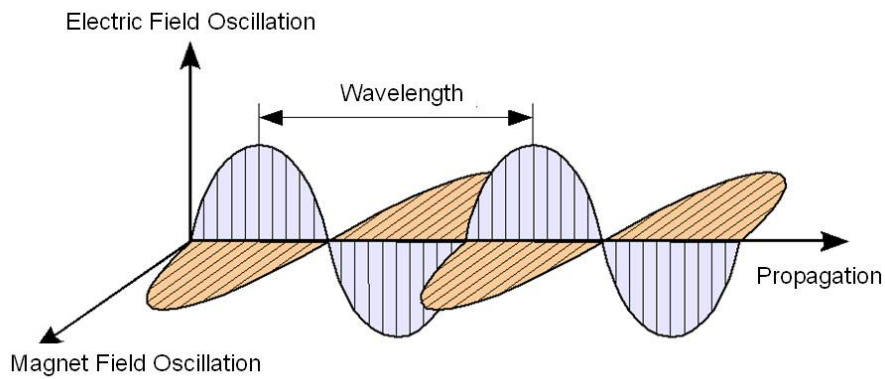
Figure 2.2: Representation of electromagnetic waves propagation [2].

In general, the propagation constant is defined as a complex number, $\gamma = \alpha + j\beta$, in which the real part represents the attenuation constant (in Np/m) and the imaginary part regards to the phase constant (β). Both attenuation constant and phase constant can be calculated according to equations 2.6 and 2.7, respectively [28, 5, 30].

$$\alpha = \omega\sqrt{\frac{\mu\varepsilon}{2}[\sqrt{1+(\frac{\sigma}{\omega\varepsilon})^2}-1]} \tag{2.6}$$

$$\beta = \omega\sqrt{\frac{\mu\varepsilon}{2}[\sqrt{1+(\frac{\sigma}{\omega\varepsilon})^2}+1]} \tag{2.7}$$

The attenuation constant corresponds to the exponential decay of the electric field magnitude as well as the power dissipated in a lossy dielectric, as shown in the figure 2.3. According to A.C. Metaxas the attenuation of the EM energy depends on the loss factor, specific for each material. This loss factor is defined as the quantity of energy loss within a dielectric material due to conduction, currents polarization, and other dissipative phenoms [3].
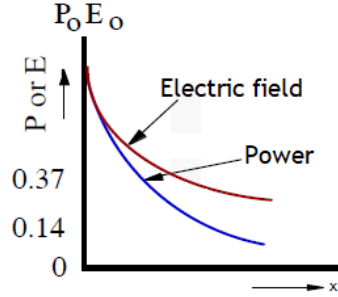
Figure 2.3: Electric field and power distribution, adapted from [3].

The distance, x, at which the amplitude of the EM field is attenuated by a value of $1/e$ is referred as the penetration depth or skin depth (in m), equation 2.8.

$$\delta = \frac{1}{\omega \sqrt{\frac{\mu \varepsilon}{2}[\sqrt{1+(\frac{\sigma}{\omega \varepsilon})^2}-1]}} \tag{2.8}$$

Therefore, as a wave travels through a lossy medium, a decreased in amplitude occurs. For example, for a wave propagating along the x-axis the amplitude of the dissipated power will exponentially decrease within a lossy medium as equation 2.9 [30, 31].

$$P(x) = P_0 \cdot e^{\frac{-2x}{\delta}} \tag{2.9}$$

where $P(x)$ represents the power at a certain depth (in W), x the penetration (in m), P_0 the incident power (in W) and δ the penetration depth [3].

2.1.2   Interaction of Electromagnetic Fields with Biological Tissues

Typically, the EM field is described by the Maxwell's equations that represents the interaction between the two vectors regarding to the electric and magnetic fields. Maxwell's equations allow the study of every single phenomenon on electromagnetic space. In turn, the propagation of an EM field through biological tissue can be expressed resorting to Maxwell's equations:

$$\nabla \cdot \vec{D} = \rho \tag{2.10}$$

$$\nabla \cdot \vec{B} = 0 \tag{2.11}$$

$$\nabla \times \vec{E} = -j\omega \vec{B} \tag{2.12}$$

$$\nabla \times \vec{H} = \vec{J} + j\omega \vec{D} \tag{2.13}$$

The interaction between EM fields and biological tissues can be classified as ionizing or non-ionizing radiations, depending on its ability to ionize matter, i.e., according to the effects that they can provoke in tissues. Ionization of the matter occurs when the EM radiation has sufficient energy per photon to cause the removal of an electron from an atom or molecule, i.e., when the energy of each photon is greater than the binding energy of the electrons, producing ionized atoms and molecules. In turn, non-ionizing radiation does not have enough energy to cause ionization of matter, having only the ability to excite the motion of the atoms and molecules or to move an electron from an occupied orbital into an empty higher energy orbital. The EM radiation frequencies higher than those corresponding to the region close to the UV of the EM spectrum is ionizing, whereas EM radiation of lower frequency than the region furthest from UV (such as visible light, IR and RF) is non-ionizing [27, 30, 32]. Figure 2.4 illustrate the ionizing and non-ionizing radiation in the electromagnetic frequency spectrum.
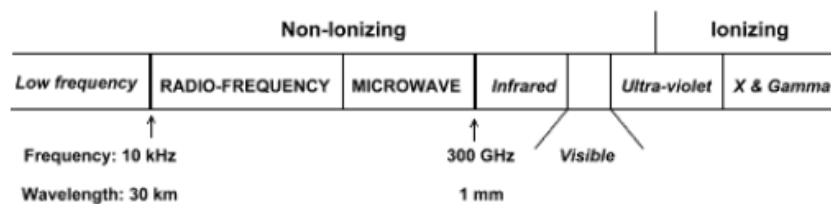
Figure 2.4: Electromagnetic frequency spectrum [4].

Biological tissues are complex aggregations of cells with similar structure and function that can be divided in four main types: epithelial, connective, muscular and nervous. Epithelial tissue covers the external and internal surfaces of the body. It consists in a single layer or multiple layers of epithelial cells between the outer surface of the skin and the basement membrane and is responsible for the human body protection, regulation of secretion and absorption of matter. Connective tissues are essentially characterized by extra-cellular material that separates cells from others and, consists in fibers and gelatinous substances that support and connect the cellular tissue to the skeleton. Muscle tissue constitutes the muscles of the body, hollow organs, cardiac muscles

and are responsible for the movement, i.e., contraction and extension function of the muscles. The nervous tissue is responsible for sensing, controlling and governing body activity. It has the function of transmitting the information by conducting signals in response to a stimulus through electric impulses from the sensorial receptors to the central nervous system and, from the central nervous system to the target organ, gland, etc. In turn, most of biochemical reactions that happen involve electrical processes [5, 30, 7, 33].

Regarding the effects on biological tissues by their exposure to EM fields, they mainly depend on the EM field frequency and magnitude. Low frequency electric fields do not have enough energy to penetrate the body significantly, they only influence the distribution of electric charges at its surface, which will cause a flux of electrical current in the body. Magnetic fields of low frequency induce the circulation of electrical currents in the interior of the body. The intensity of these circulating currents depends on the intensity of the magnetic field and on the length through which current flows, figure 2.5 [5, 33].
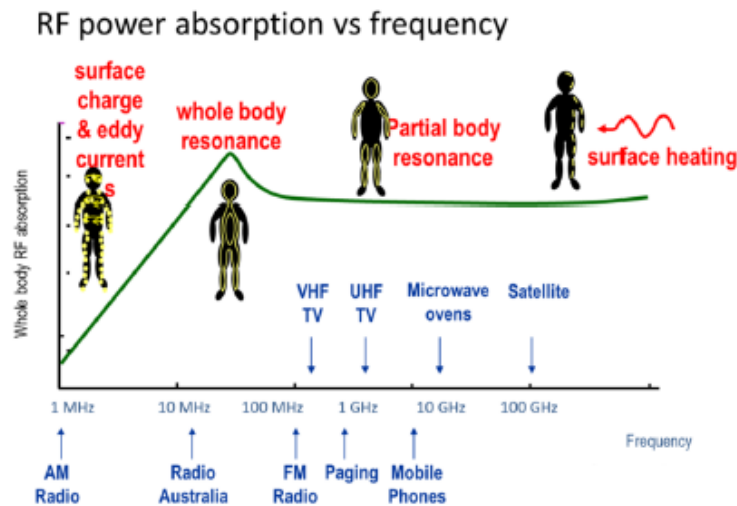
Figure 2.5: Diagram illustrating approximate frequencies for power absorption [5].

Radiofrequency fields can penetrate small distances within the body and its energy is absorbed by the tissues causing the agitation of the atoms and molecules. This friction associated to the rapid movement of molecules generates an increase of the local temperature, also denominated as "Joule effect", in the biological tissue. As previously mentioned, current density (J) is given by the product between electric conductivity (σ) and the electric field intensity (E) hence, it is possible to understand that the higher the current that flows within the body, the more intense will be the friction between molecules and atoms and, consequently, the higher the temperature reached over a certain time, affecting the biological tissues in terms of possible necrosis and cell death [4, 7, 33].

To study the interaction of the EM fields between the body tissues it is important to know that the propagation of an EM wave is affected by the dielectric characteristics of the medium: permittivity, conductivity and permeability. The body tissues are not magnetic materials, which

means that their magnetic permeability is 1. On the other hand, the permittivity and conductivity are specific for each type of tissue and are frequency-dependent.

Generally, in the radiofrequency range, the relative permittivity (ε_r) is inversely proportional to frequency, i.e., the smaller the permittivity, the higher the frequency and vice versa, figure 2.6. The resistivity, which is the reciprocal of conductivity, tends to gradually decrease with the increasing of the frequency at low frequencies and, tends to decrease rapidly for the high frequencies, figure 2.7 [28, 30, 6].
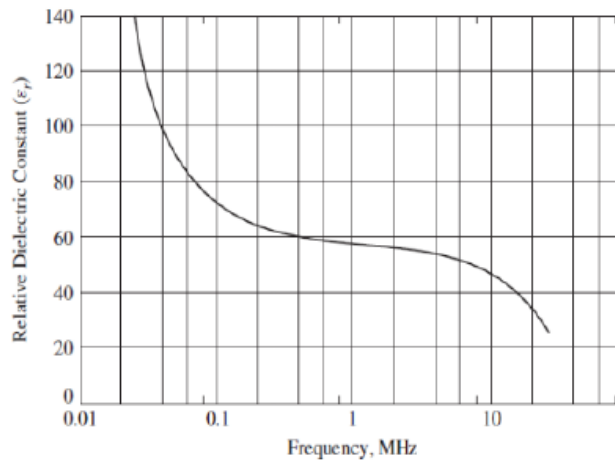
Figure 2.6: Relative dielectric constant (or relative permittivity) distribution of human tissues [6].
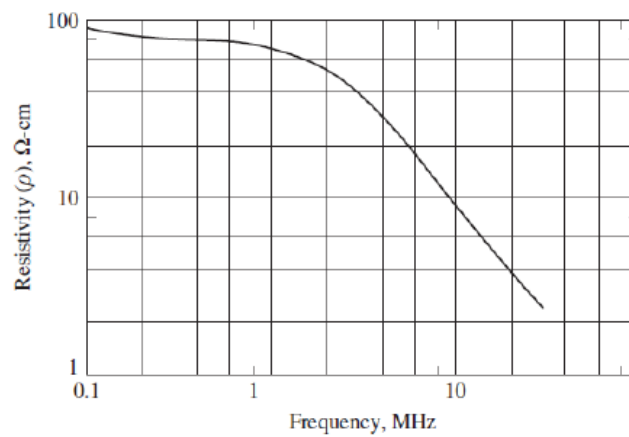
Figure 2.7: Resistivity distribution of human tissues [6].

2.1.3 Electromagnetic Radiation Exposure Standards and Dosimetry

The process of developing standard protection values for the human health exposure to EM fields constitutes a very complex procedure that started from the realization of an extensive scientific

research including the studies that describes its thermal and non-thermal effects, short and long-term exposures, biological and health effects [34].

In this sense, several organizations work to establish standards that limit the acceptable human exposure to electromagnetic radiation. Standard limits refer to the exposure levels that are harmful or are considered less hazard to the human health. These limits may be referred by different organizations as recommendations or guidelines for exposure limits or are named as permissible exposure levels or maximum permissible exposure (MPE). MPE limits depend on the frequency range of the EM fields. There are several variables used for the expression of the MPE limits such as the magnetic flux density, current density, specific absorption rate (SAR) and power density (in W/m^2) [34, 35].

Specific absorption rate (SAR) is defined as the amount of power absorbed per unit mass of a body or part of the body and, is expressed in W/kg. SAR represents a dosimetry measurement of how much dose is absorbed by humans with different characteristics such as body size, allowing a good prediction of the thermal effects. There are two alternatives used for SAR evaluation from either electric field or temperature measurement. Therefore, SAR can be determined by the following equations:

$$SAR = \frac{\sigma \cdot |E^2|}{2\rho}, \tag{2.14}$$

where E is the amplitude of the electrical field (in V/m), σ the conductivity (in S/m), and ρ is the tissue density (in kg/m^3) [30, 7, 35, 36].

$$SAR = c_h \frac{dT}{dt}, \tag{2.15}$$

where c_h is the tissue specific heat (in $J/(kg.°C)$) and dT/dt is the temperature rise in the tissue during a t time (in seconds) of irradiation [5].

Regarding to the SAR values, they can be classified in two types: the whole-body SAR average and local tissue SAR average. Both types are averaged during a certain period of time and a tissue mass value over 1 or 10 g is considered. Averaging the absorption over a large amount of tissue gives less reliable results compared to that obtained when, for example, 1 g SAR is considered since it involves a more precise and localized RF energy absorption and, consequently, a better measure of SAR distribution [5, 7].

The whole-body SAR average should not exceed 0.08 W/kg, while the limit, according to the stipulated by IEEE, is 1.6 W/kg (reference in North America) averaged over 1 g and 2 W/kg averaged over 10 g is the limit stipulated by ICNIRP, accepted in Europe. Although these limits constitute reasonable values for RF radiation exposure, due to the fact that both are calculated over different values of mass, they cannot be directly compared. Figure 2.8 presents several SAR limit values for some exposure recommendations [5, 7].

SAR Limits for RFR

Standard	Frequency Range	Whole-Body SAR (W/kg)		Local SAR in Head (W/kg)		Local SAR in Limbs (W/kg)	
		Public	Occupational	Public	Occupational	Public	Occupational
ARPANSA	100 kHz–6 GHz	0.08 (6)	0.4 (6)	2 [10] (6)	10 [10] (6)	4 [10] (6)	20 [10] (6)
TTC/MPT	100 kHz–6 GHz	0.04 (6)	0.4 (6)	2 [10] (6)	8 [10] (6)	—	—
Safety Code 6	100 kHz–10 GHz	0.08 (6)	0.4 (6)	1.6 [1] (6)	8 [1] (6)	4 [10] (6)	20 [10] (6)
ICNIRP	100 kHz–6 GHz	0.08 (6)	0.4 (6)	2 [10] (6)	10 [10] (6)	4 [10] (6)	20 [10] (6)
FCC	100 kHz–6 GHz	0.08 (30)	0.4 (6)	1.6 [1]	8 [1] (6)	4 [10]+	20 [10] (6)+
NRPB	100 kHz–6 GHz	0.4 (15)		10 [10] (6)		20 [100] (6)	
ANSI/IEEE	100 kHz–6 GHz	0.08 (30)	0.4 (6)	1.6 [1] (30)	8 [1] (6)	4 [10] (30)+	20[10] (6)+

Note: ( ) Averaging time in minutes. [ ] Averaging mass in grams. + In hands, wrists, feet, and ankles.

Figure 2.8: Human's SAR Limits for RFR, adapted from [7].

As previously mentioned, it is possible to relate the SAR with heating temperatures, for example, a SAR of 1 W/kg is equivalent to a heating rate of less than 0.0003 °C per second of a muscle tissue, which correspond to a temperature increase about 1 °C after 3333,33 seconds. In addition, for a SAR of 4 W/kg a tissue disruption, is still reversible. Permanent effects were found for values of SAR above 5 W/kg [5, 7].

Although SAR constitutes a good tool to determine the effects of EM fields in tissues, sometimes its measure is not enough. Clearly, high SAR values can be associated, for example, with the proximity of the person to the radiation source, which in turn indicates more or less danger to humans. However, most of the times it is necessary to have a better understanding of what actually happens in biological tissues. For that, it is important to know the time of exposure of the tissues to obtain the desired temperature increase, without damaging. Moreover, it is necessary to obtain the increase of tissue temperature to conclude if the radiation effects are hazard for humans or not [5].

2.1.4 Effects of Electromagnetic Radiation Exposure on the Human Health

Since electromagnetic fields naturally occur in nature and humans are inevitably exposed to electromagnetic radiation, several studies have been developed with aim of set safety standard values to radiation exposure so that human health would not be affected. Nowadays, there is no scientific

evidence that exposure to electromagnetic radiation at values above standardized levels is harmful to health. However, this fact does not guarantee that exposure to low frequency EM fields is harmless to the body [30, 37]. The interaction of RF fields with living tissues can be classified in: molecular, sub-cellular, cellular, organ, or system level, as well as the entire body. Moreover, biological effects due to exposure to RF fields are differentiated in three levels: high-level or thermal effects, moderate-level or a-thermal effects and, low-level or non-thermal effects [7].

Thermal effects may occur from the exposure to RF fields exceeding frequency values in the frequency range between 100 kHz to 10 GHz. The extension of heating lesions depends on some factors such as the intensity and frequency of the field and also the balance between the amount of energy absorbed per unit of time and body or tissue ability to dissipate heat. The a-thermal effects are defined as the amount of charge generated in excess by the human body that is not dissipated through the typical thermoregulation mechanisms such as the blood flow and sweating. When the body is subject to an EM field, a normal phenomenon of basal metabolic rate (BMR) occurs. In turn, there are some thermal effects associated to that of thermoregulation mechanisms, apparently harmless to human health. Non-thermal effects are those that do not originate changes in temperature when the body is exposed to radiation [30, 34].

There are quite a few studies that demonstrate the effect of exposure to weak RF fields on hormonal regulation. Some of these were performed with the aim of examining whether changes in the production of melatonin, a hormone that regulates the circadian rhythm, occur. However, most of the studies provide no consistent evidences of the adverse effects of the exposure to weak RF fields in the hormonal system in humans [34].

Regarding to cancer diseases, several studies were developed that investigated the development of the incidence of brain tumors over time in children and adolescents. These do not reveal any relation between the increased incidence of the disease after the introduction of mobile phones. With respect to leukemia, lymphoma, salivary gland tumors and other tumors the existing studies do not suggest an increased risk of the disease incidence. In addition, previous studies demonstrate no increased risk of brain tumors associated with the usage of mobile phones up to 10 years. Although none of these studies indicated a reliable increase in risk, they warn to the possibility of a small to moderate risk increase associated to the frequent use of mobile phones, especially for glioma and acoustic neuroma [1, 34].

Another effect that is likely to result from the exposure to RF fields in the frequency range up to 10 MHz is the excitation of nervous tissue, when the electric fields are induced above certain intensities in the body [34].

Furthermore, the effects of radiofrequency fields exposure on cell cultures as also been investigated. Mostly of the performed researches did not provide evidence of any harmful effect of radiofrequency field exposure on isolated cells and tissues at an intensity level below the one that provokes the thermal effects [20].

2.2 Hyperthermia

Thermal ablation refers to the destruction of biological tissues by means of hyperthermia, i.e., by application of heat at temperatures at which cells do not survive. Hyperthermia is defined as the complete overheating (systemic) or partial (local or regional) of biological tissues. In hyperthermia, generally, temperatures above 41 °C are used that cause blood vessel dilation and, consequently, increasing of blood perfusion. At temperatures above 46 °C, an irreversible cell damage begins, the response to thermal shock is intensified, and after approximately 10 minutes of exposure, a significant cell population death can occur. The time required to achieve cell death between 46-52 °C is reduced and is possible that microvascular thrombosis and hypoxia occur. Temperatures above 60 °C cause a fast protein denaturation and the melt of plasma membrane that allows cell survival [20, 8, 28].

The concept of hyperthermia for treating tumors has been explored after observations that cancer cells exhibit greater sensitivity to heat than normal cells. Ablation or hyperthermia at high tumor temperatures is defined as the direct application of chemical or thermal therapies to a tumor to achieve its substantial eradication or destruction. The aim of tumor hyperthermia ablation is to destroy the entire tumor using heat to kill malignant cells with a significant margin of healthy tissue to prevent local recurrence [20, 19, 8].

During the thermal ablation of tumors, the tissue is killed "in situ" and is subsequently absorbed by the body, during several months. This can be performed by different ways such as percutaneous, laparoscopic and laparotomy. However, the most recurrent is the percutaneous approach once it has many advantages over the others. This is the least invasive procedure, can be performed on an outpatient basis, requires only patient sedation, is relatively inexpensive, and can be repeated whenever necessary to treat possible tumor recurrences. With the laparoscopic technique, a tumor can be fully visualized from a high-frequency transducer positioned directly on the target tissue surface. This technique allows the visualization (and treatment) of small tumors that cannot be detected in other imaging techniques. In addition, tumor extraction can be achieved more accurately, but, on the other hand, it is a more invasive approach, with many associated complications, and a higher cost [20, 9].

Thermal ablation of tumors is becoming increasingly important for the treatment of many types of cancer such as cancer of the breast, liver, kidney, lung, bone, etc. In this sense, several different hyperthermia ablation techniques based on electromagnetic radiation have been developed, such as ultrasound, radiofrequency and microwave ablation [17, 8].

2.3 Hyperthermia Techniques

As previously mentioned, hyperthermia consists of two different processes: the systemic, which constitutes the whole-body heating (whole-body treatment), and the local (or regional), where only part of the organism is heated. Thermodynamically, these two types of heating differ in their

energy consumption. In addition, they present different physiological limitations: systemic treatment modifies the whole physiology of the organism, which may limit the absorption of energy applied and body temperature. While systemic treatment is based on heating the blood, local hyperthermia is the direct heating of a tissue. In other words, in systemic treatment, the blood acts as a heating medium, distributes heat to the target tissue and heats it, while in the local treatment the blood remains at body temperature during heating, functioning as a cooling medium (heatsink) to the locally heated tissue (figure 2.9) [8].
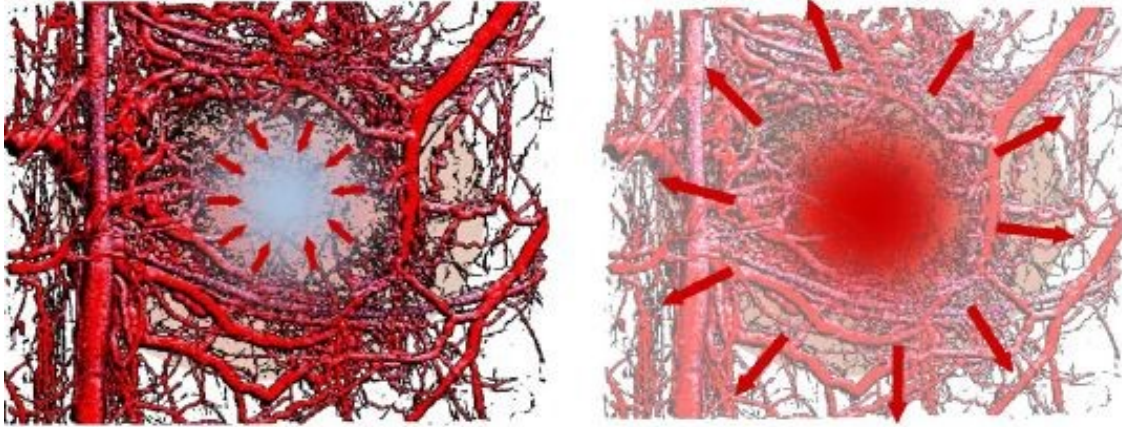
Figure 2.9: Heating methods by hyperthermia, systemic and local, respectively. The tumor warmed by the blood, in the systemic treatment, reaches the thermal equilibrium after some time; while in the local treatment, because the body is at a different temperature from the target tissue, there are constant heat exchanges, and consequently there is no thermal equilibrium between the systems [8].

There are two direct methods for the practice of systemic hyperthermia: the extracorporeal, where the blood is heated outside the body, and the intracorporal, where blood is warmed "in situ" in the body, being the extracorporeal method the least used. In most cases, the capillary bed of the subcutaneous area is heated by conduction (e.g., warm bath) or by radiation (infrared, radio-frequencies, etc.) by extracorporeal blood heating [8].

Systemic hyperthermia treatment can be performed in several ways such as heating by steam, water or radiation (figure 2.10). The human body is entirely heated, being that the thermal distribution happens in a homogeneous and controlled manner [8].

The practice of local hyperthermia can be done by convection, conduction or by electromagnetic radiation. The most recurrent technical solutions for local hyperthermia have been explored, essentially, from the discovery of electromagnetic radiation heating, since electromagnetic waves are able to penetrate the body in depth. However, other practices for local heating, such as contact heating, deep heating, or immersion of a part of the body in hot water are also used (figure 2.11) [8].

Both systemic and local hyperthermia represent two main groups of heat therapies for tissue heating, both are involved in different physiological actions that support different mechanisms of
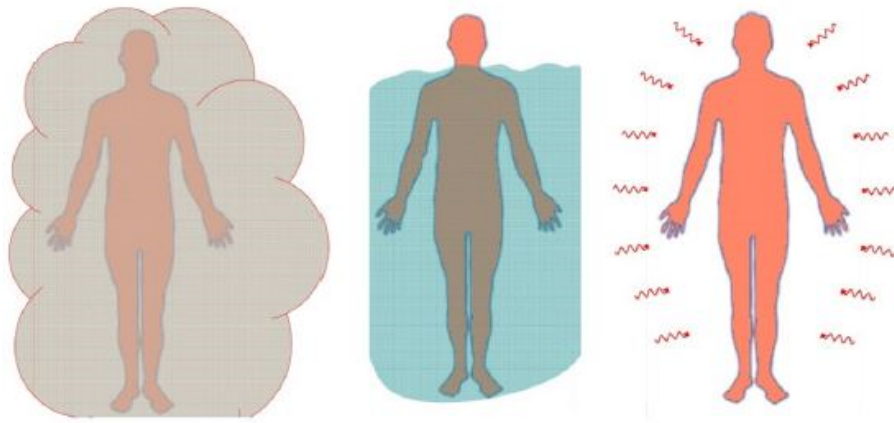
Figure 2.10: Different methods of systemic heating, such as by steam, immersion of the body in hot water and radiation, respectively [8].
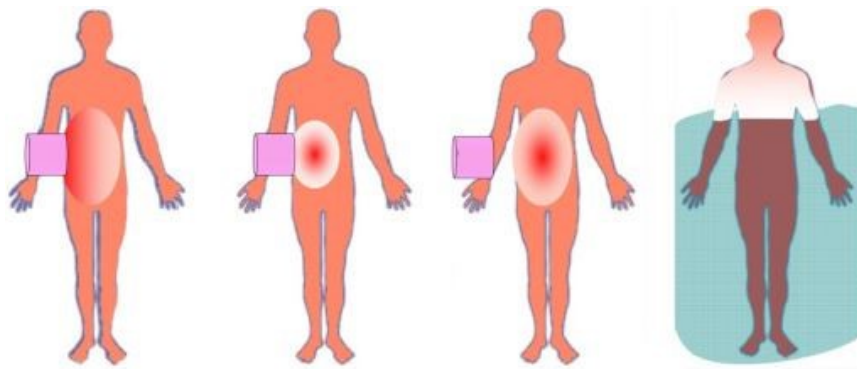
Figure 2.11: Different methods of local heating, such as by contact, deep, radiation and immersion of the body in hot water, respectively [8].

reaction in the body. The way they produce energy, area, type of energy supply, being more or less invasive, frequency of electromagnetic waves, as well as their medical applications and combination with other methods are the factors that define and make these thermal therapies unique [8].

2.4 Electromagnetic Radiation in Hyperthermia Ablation Techniques

Regarding to the application of electromagnetic radiation in hyperthermia ablation, three distinct groups of techniques can be considered according to the frequency range, ultrasound, radio frequency and microwave intervals [30].

2.4.1   Ultrasounds

The High Intensity Focused Ultrasound (HIFU) technique is a noninvasive ablation method that relies on the convergence of ultrasound beams from an external source to produce a focal zone of heating. At frequencies, typically between 0.8 MHz and 10 MHz, ultrasound waves can penetrate soft tissues to produce physiological effects, being that as ultrasound waves propagate in depth through tissues, they are progressively absorbed, and their energy is converted to heat. Otherwise, the ultrasound field focus limits the heating volume of the tissue to only a few cubic millimeters, causing necrosis by coagulation of the cells (lesion), without affecting the adjacent tissues (figure 2.12) [19, 38].
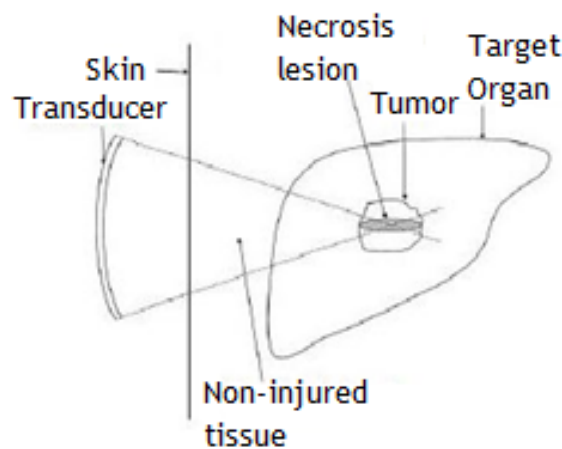
Figure 2.12: Schematic representation of a lesion caused by the HIFU procedure [8].

The goal of HIFU treatment is to heat an isolated tissue volume up to 50 °C and maintain that temperature for 1 second or longer to cause its total ablation. A complete treatment consists of overlapping lesions until the entire volume of the tissue is covered. In this way, HIFU procedures can take hours to complete and require precise control over the treatment zone, during this time. For this reason, the HIFU technique was first applied in areas of easy access, without substantial movements of respiration, such as in benign fibroids in the uterus and breast and benign hyperplasia in the prostate [20, 19].

The HIFU technique, as a method for producing local hyperthermia, has some advantages compared to other methods, such as radiofrequency or microwave ablation. HIFU is a noninvasive method that uses non-ionizing radiation, which means it can be safely repeated because it has no long-term cumulative effects. The ability to cause cell death in a volume of tissue far from the source of ultrasound makes this technique a viable option for the development of non-invasive surgical treatment tools. On the other hand, sound waves do not easily propagate through air or solid surfaces consequently, the HIFU technique presents a problem at the air-tissue interface where the sound does not penetrate the tissue but is reflected. In addition, high densities of bone composition also cause a reflection of the energy at the tissue-bone interface, causing excessive tissue heating near the bone. Moreover, the small amount of energy that penetrates the bone

can produce excess heating in the bone itself, due to its high coefficient of absorption. Another disadvantage is the prolonged treatment time, especially for tumors of larger volume [39, 40].

2.4.2 Radiofrequencies

Radiofrequency energy is seen as the safest of many cancer therapies once it is absorbed by biological tissue as heat. Regardless of the heat source, cells die when they reach a determined temperature. The main effect of radiofrequency ablation in tumors occurs because the absorption of electromagnetic energy induces thermal effects on the tissue. The ability to efficiently produce ablation is based on the energy balance between the conduction of localized radiofrequency energy and the convection of heat from the blood, lymph, or extra and intracellular fluid circulation [8].

Radiofrequency ablation consists of converting radio waves, between 375-500 kHz, into heat through ionic vibration. The passage of alternating current of high frequency vibrates the molecules of the tissues and thus, the friction between molecules results in a localized temperature increase. The higher the current, the stronger the movement of the ions and, consequently, the higher the temperature reached, over a certain period of time, leading to coagulation necrosis and cell death [19, 8].

The properties of ablative tissues and normal tissues are quite different and therefore should be considered for ablation. In radiofrequency ablation, the properties of the most important tissues to be considered are: electrical conductivity and thermal conductivity. It is important to be aware that tissue resistance is inversely proportional to conductivity. High electrical conductivities (i.e., low resistances) allow higher current flow and higher power to be applied by the radiation source, while low electrical conductivities (high resistances) inhibit current flow. Thermal diffusion (or dissipated power) of the tissues should also be considered since this is the factor that determines how rapidly the heat can be transferred from the target heating zone to the surrounding tissues [17].

The thermal, electrical and mechanical properties of the tissues vary with numerous factors but are mainly influenced by the water content and cellular composition. Heating a tissue at temperatures close to or greater than $100\,^\circ$C causes boiling of water and release of gases, leading to tissue dehydration and significant changes in electrical properties. Thus, above $100\,^\circ$C the radiofrequency current hardly passes through the tissues because the amount of water required for the ion fluid has evaporated. These are the factors that cause the characteristic increase of the impedance during the treatment by radiofrequency hyperthermia. Furthermore, as previously said, heating tissues above $50\,^\circ$C causes irreversible changes in cells. It is possible to determine the heat flow of the ablation source from the following equation:

$$Q_{ext} = J \cdot E = \frac{J^2}{2\sigma} = \frac{\sigma E^2}{2}, \qquad (2.16)$$

where Q_{ext} represents the heat flux from the ablation source, J the current density (A/m), E the electrical field intensity (V/m), and σ the electrical conductivity (in S/m) [20, 17].

Compared to other methods, the radiofrequency technique has some advantages. Radiofrequency ablation systems may be simpler and cheaper to develop and are suitable for small volume therapy since the energy deposition of radiofrequency waves is rapidly attenuated with increasing distance to the source. Otherwise, radiofrequency ablation has a limited extent of induced cell necrosis, or incomplete necrosis near blood vessels, and ablation zones generally do not exceed four centimeters unless the ablation probe is repositioned for second treatment [30].

2.4.3   Microwaves

Microwave ablation refers to all methods that use electromagnetic radiation for the destruction of tumors with frequencies of at least 900 MHz. It is a special case of dielectric heating where the dielectric material is the tissue. Dielectric heating occurs when an alternating electromagnetic field is applied to the material. In tissue, the heating takes place by the electromagnetic field that forces the movement of water molecules. The bonds between the water molecules tend to oscillate out of phase with the applied fields, some of the applied electromagnetic energy is absorbed and converted to heat. Thus, the tissues that most absorb microwave radiation are those with the highest percentage of water, while lower heating occurs in tissues with low water content [17, 10].

In microwave ablation, temperature is a measure of how fast the water molecules move, and the more vigorous their movement, the higher the final temperature reached. Thus, electromagnetic waves heat matter by shaking the water molecules in the surrounding tissues, producing friction and heat, inducing cell death by coagulation necrosis [10].

For microwave ablation, the most important properties of the tissues to be considered are relative permittivity (or dielectric constant) and conductivity. Relative permittivity, although a term that varies significantly with temperature and frequency, is a measure of how well a material accepts the electric field and is measured as a function of vacuum permittivity (ε_0). Relative permittivity determines the wavelength of the field applied at a given frequency that affects how well the energy will propagate through tissue. Conductivity refers to the spin-related effects of water molecules, and the property determines how well a tissue is capable of absorbing microwave energy. As mentioned before, high conductivity tissues are made of a high-water content and therefore easily absorb energy, whereas low conductivity tissues have a reduced water content allowing the propagation of the microwaves through tissues [17].

The heat generated by the microwave ablation source can be deduced from the following equation:

$$Q_{ext} = \frac{\sigma E^2}{2} \tag{2.17}$$

As advantages, the microwave technique shows evidence that it is capable of propagating through materials of low or none conductivity, the ablation process is faster and higher temperatures can be achieved. In addition, the microwave energy can be used by a multiple application probe, i.e. multiple radiation emitting antennas can operate simultaneously and continuously, close to one another or in separate locations which allows obtaining more focused heat, indicated for organs of high vascular perfusion or near vascular heat sinks. The lack of electrical stimulation, associated to the radiofrequency technique, allows the elimination of possible lesions caused by the mass electrodes and is therefore a less painful procedure. On the other hand, the microwave energy can overheat the cable used to transfer energy from the generator to the applicator. In this sense, since the transmitted energy is limited, it is necessary to use a cable with a cooling system, in order to prevent thermal injuries in normal tissues [30].

2.5 Examples of Ablation Systems for Hyperthermia Based on Electromagnetic Radiation for Therapeutic Purposes

To overcome the problems of desiccation and carbonization of tissues and a limited tissue coagulation radius around the needle electrode for ablation, three companies in the United States, producers of ablation devices, performed experiments with different models of needle electrodes and radiation sources at different frequencies. Each marketed device uses a model of different radio frequency needles, different voltage sources, and algorithms from the sources that vary from each other [9].

One of the manufacturers produces a system with two retractable needle electrodes (Model 70 and Model 90 Starburst XL Needles; RITA Medical Systems). Needle electrodes consist of insulated 14-gauge or 15-gauge needles which house seven or nine multi-length bend electrodes, respectively. These devices assume a shape similar to a "Christmas tree" (figure 2.13), where the electrodes have a length and diameter of approximately 3 and 5 cm, respectively. Four of the electrodes are hollow and contain thermocouples at the tips that are used to measure the temperature of the adjacent tissue. The electric current generator generates powers of 50 W and 150 W, operating at a frequency of 460 kHz. After the needle is inserted, at the desired location, and the electrodes implanted up to approximately two-thirds of their length, the generator is turned on and runs automatically from a program. The program starts the generator at 25 W and gradually increases the voltage to the peak power in 30-120 seconds. In addition, the program allows monitoring the temperature at the tip of the electrodes and maintains peak power until the temperature exceeds the desired temperature. After the desired temperature is reached, the electrodes are advanced slowly for complete implantation while maintaining the temperature. When the electrodes are completely implanted, the program maintains the constant temperature by regulating the voltage. Depending on the fabric dries, the amount of power required to maintain the constant temperature decreases [9].

Another radiofrequency ablation system consists of curved electrodes and isolated 14-gauge insulated needles housing 10 retractable curved electrodes which, when implanted, assume an
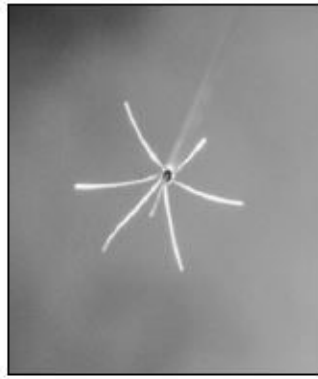
Figure 2.13: Picture representing the configuration in "Christmas tree" of the needle electrode tips constituting the RITA device; Medical Systems [9].

umbrella like-shape (LeVeen Needle Electrode; Radiotherapeutics) (figure 2.14). Electrodes of different sizes, between 2 and 3.5 cm in diameter, are manufactured, with 3.5 cm electrodes being the most recurrent. The alternating current generator operates at a power of 100 W and at a frequency of 480 Hz. For ablation, the device uses two ground terminals placed on the patient's thighs. The tips of the radiofrequency needles are introduced into the patient to the target tissue and the bend electrodes are implanted for full extension. The generator is switched on and immediately set to 30 W and, every 60 seconds the power is increased by 10 W until it reaches the peak power (*90 W*). The device is maintained at its peak power for 15 minutes, or until "impedes out", i.e., a rapid increase in impedance stops the current flow . If the device impedes out, it shuts off for a period of 30 seconds and then, a new cycle restarts until it reaches a peak of about 70% of the maximum reached at the time of the impairment. Otherwise, the device shuts off when it reaches the maximum power peak for 30 seconds, and restarts until it reaches the peak again or until a possible impediment of alternating current passing occurs [9].
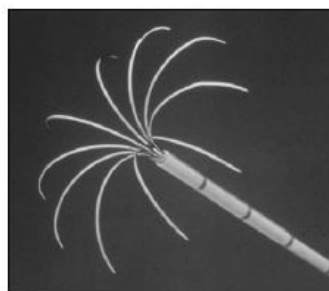
Figure 2.14: Picture representing the "umbrella" configuration of the needle electrode tips constituting the device developed by Radiotherapeutics [9].

According to Golberg et al. and Lorentzen et al., radiofrequency needle systems composed of a cooling system produce greater ablation than the others. In this sense, a third radiofrequency ablation device emerged consisting of a system of isolated hollow needles with exposed tips and

variable length (2-3 cm) (Cool-Tip radiofrequency electrode; Radionics). The tip of the needle is
shut and contains a thermocouple that records the temperature values of the adjacent tissue. The
needle extremity is composed of two channels that allow it to be filled with fresh water. To increase
the size of the ablation zone, the manufacturer chose to place three of the cooled needles grouped
in parallel with a common axis (figure 2.15). The generator has a peak power of 200 W, is the
most powerful of the three, and operates at a frequency of 480 Hz. For ablation, 4 mass terminals
are placed on the patient's thighs. The electrode tips are introduced into the patient to the desired
zone of the tissue to be treated. To begin the procedure, a program automatically increases the
power gradually for 1 minute until the maximum peak (200 W) is reached, keeping it to the point
where the impedance increases 20 Ω from the initial level. Afterward, the power is automatically
reduced by 10 W for 15 seconds and restored to its maximum until the impedance increases again.
If the power is not maintained for more than 10 seconds without the impedance increasing, the
power is reduced for subsequent cycles in order to minimize impedance increases [9].

Figure 2.15: Picture representing the configuration of the tips with cooling system of the RF
electrodes developed by Radionics [9].

Simon et al., developed a study to evaluate the ablation zone and histological characteristics
of microwave ablation using an ablation system available for use in humans in the United States
(Figure 2.16). This system consists of a micro-wave antenna (14.5-gauge) which uses a gener-
ator capable of generating power in the order of 60 W at a frequency of 915 MHz. Due to the
characteristics of the electromagnetic waves, for ablation, this device does not require the use of
mass terminals, thus alleviating the burn problem associated with mass electrodes. In addition, the
temperatures of the tissues under the antenna can be measured separately through a thermocouple
[10].

Regarding to the HIFU technique, ultrasound energy can be supplied from interstitial or extra-
corporeal devices. Target tissues such as the breast, abdomen, brain or limbs are usually treated
through the use of extracorporeal HIFU devices. Treatments through the skin require the need
for a suitable acoustic window on the skin that provides a path of propagation to the beam so
that it is not affected by the intervening gas. For this, a coupling of the ultrasound energy to the
surface of the skin should be done through a coupling gel, a water balloon or other suitable liquid

Figure 2.16: Picture showing microwave applicators available for percutaneous tumor ablation (Vivant Medical, Mountain View, Calif.) [10].

medium. An example of an extracorporeal HIFU device is the Exablate Neuro (Insightec Ltd, Israel) which consists of a medical device that uses high intensity focused ultrasound along with magnetic resonance imaging (MRI) technique to accurately target and treat a deep target tissue. This concentrates 1024 ultrasound waves to generate sufficient heat in order to cause ablation of the tissue, at approximately temperatures between 65-85 °C. During planning and treatment, the patient lies in a bed, inside a magnetic resonance chamber. MRI provides a high-resolution view, allows planning of patient-specific treatment, and continuous monitoring of the entire ablation procedure. Real-time thermal feedback allows the user to control and adjust the focused ultrasound to ensure total ablation of target tissue [41].

Other HIFU ablation techniques have emerged with the development of interstitial devices. Prat et al. have developed an ultrasound applicator for the treatment of biliary intraductal tumors. The applicator consists of a stainless-steel tube 8 cm long and 3.8 mm in diameter with a copper cone tip at the end (figure 2.17). The active part constituting the tip is a flat piezoceramic transducer, 3x10 mm^2, water-cooled, operating at frequencies between 5 MHz or 10 MHz depending on the depth to be achieved. Cooling with water prevents overheating of the transducer and facilitates acoustic coupling between the transducer and the tissues. In addition, a hub is placed, opposite to the active part, for the remote control of the rotational movement of the applicator at the tip of the probe. The angle of rotation of the probe is controlled by a micrometer screw. Electrical wiring is protected by a 50 Ω coaxial cable. For temperature monitoring during treatment, a thermocouple is attached to the outer face of the transducer. The electrical energy is supplied through a generator of sinusoidal wave, in continuous mode, through a power amplifier. The generator is controlled by a timer to allow the automation of signal emission and cut-off. Another example of an interstitial device for the treatment of esophageal tumors consists of a piezoceramic transducer, 15x8 mm, using 10 MHz frequencies, mounted on a flexible cable, 10 mm in diameter and 80 cm in length. This device operates at intensities between 12-16 W/cm^2 for an exposure time between 5 and 20 seconds [42, 11].

Trans-rectal devices for the treatment of benign and malignant prostate tumors have also been developed for ablation by the ultrasound technique. Examples of such devices are Ablatherm (Edap Tchnomed, France) and Sonablate (Focus Surgery, USA). Both systems incorporate therapy and imaging transducers mounted on the tip of a trans-rectal probe. The clinical objective of
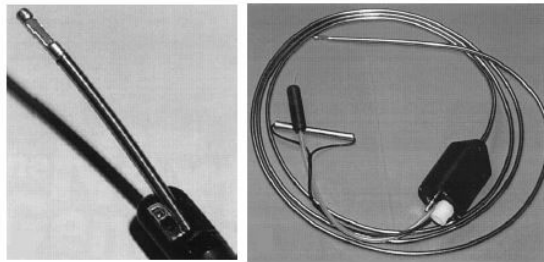
Figure 2.17: Picture representing the configuration of the HIFU applicator, on the left; Picture showing the general device configuration, on the right [11].

both systems is to cause total ablation of the prostate. In Ablatherm, the lesion length varies by ultrasound power adjustment at predefined levels, while in the Sonablae two different layers of injury are created, the deepest layer being created by a longer focal length than the most superficial layer. The different focal distances are reached by the rotational movement of the transducer, since the different sides have a different geometry. Sonablate users are still able to vary the acoustic output power of the probe [21].

2.6 Conclusions

From the review presented here it is possible to understand that to study the interaction between electromagnetic radiation and biological tissues is important to know the dielectric properties of the tissue that is exposed to radiation. In addition, it must be taken in account that these dielectric properties are frequency-dependent and, can be also influenced by some other factors such as temperature which, in turn, can affect the biological systems.

With respect to the effects of biological tissues exposure to electromagnetic radiation is important to understand that despite there is no relevant scientific evidence that shows adverse effects on human health as a result of low radiofrequency fields exposure, there is no guarantee that exposure to weak electromagnetic fields is harmless to human body. However, the exposure to high radiofrequency fields is likely to lead to some prejudicial effects on biological tissues since that can provoke the heating of the tissues and, consequently, an increase of temperature.

Concerning thermal ablation, this can be defined as the direct application of chemical or thermal therapies to a tissue to cause its eradication or substantial destruction. Thus, hyperthermia ablation refers to the complete (systemic) or partial (local or regional) destruction of a biological tissue by the application of heat. The ablation process can be performed in several ways such as percutaneous, laparoscopic or laparotomy. However, the most frequent is the percutaneous approach, due to the fact that it is less invasive and therefore less costly to the patient.

Regarding to the heating methods used for hyperthermia, two main processes for ablation can be considered: the systemic and local treatment. As can be seen, both constitutes large groups of treatment alternatives, which are involved in different physiological actions and support different

reaction mechanisms. Thus, a wide variety of different heat generation/application techniques can be used for heating the tissues. However, the way energy is produced, the location, area, type of energy distribution, being more or less invasive, the frequency of electromagnetic waves, as well as the medical application according to the patient health are factors that combined with other methods characterize each of the heating therapies, and which will determine the specific type of therapy to be used.

For the specific case of hyperthermia ablation based on electromagnetic waves for the treatment of tumors, it is possible to understand that, first, the techniques can be classified according to the frequency range, ultrasound, radiofrequency or microwave. In addition, it is possible to understand that the purpose of these techniques is to destroy all cancerous tissue as well as a significant margin of the surrounding normal tissue, to prevent a possible recurrence of the tumor. However, despite being technologies that demonstrate good clinical practice for treating tumors, they are relatively recent technologies that need to be better understood, especially due to the impact they may have on the human body. Thus, it is wise expecting for future developments and new clinical implementations that may help improve the treatment of patients with this disease.

Chapter 3

Simulation Methods of Tissues Heating by Electromagnetic Radiation

Humans maintain their body temperature relatively constant, about 37 °C, which can vary in a range between 36.1 °C and 37.2 °C. This thermoregulation is an example of a negative feedback system, which gives the body the ability to maintain a stable temperature (in thermal equilibrium), even when the ambient temperature is not constant. In humans, the maintenance of a specific value of body temperature is controlled in the hypothalamus through thermoregulatory mechanisms, such as transpiration, tremors and movement of blood vessels (vasodilatation or vasoconstriction), which regulate body temperature around 37 °C. A small area in the anterior part of the hypothalamus senses slight increases in body temperature through changes in blood temperature. As a result, mechanisms that cause an increase of heat losses, such as sweating and vasodilation, are activated and body temperature decreases. On the other hand, a small part of the posterior area of the hypothalamus can detect slight decreases in body temperature, which initiate an increase in muscle activity and induce constriction of the blood vessels, leading to a gain of heat and consequently to a rise in body temperature [43, 44].

3.1 Simulation of Tissue Heating by Electromagnetic Radiation

The exposure of the human body to electromagnetic fields is a current subject and several studies have been carried out that show reliable results of the effects of this exposure in human models through numerical methods and simulations [25].

Heat exchanges between the environment and the skin, and between tissues, occur through mechanisms of radiation, convection and conduction. Radiation is the gain or loss of heat in the form of infrared energy between two objects that are not in physical contact. It is a process that occurs at the outermost layer of the skin (epidermis), as the heat that is absorbed from the sun beams, hot beach sand, hot coal, etc. On the other hand, the heat can also be emitted by the body by radiation [43, 44].

Concerning the heat transfer in tissues, it includes some relevant mechanisms such as tissue conduction, convection, metabolic heat generation and storage of thermal energy. Conduction is the exchange of heat between objects that are in direct contact, for example, between the skin and the inner tissues of the body (e.g., breast tissue). Regarding to the tissue conduction, the conductive heat flux (q_i) is proportional to the gradient of temperatures, where the proportionality constant is defined as the thermal conductivity (k), equation 3.1.

$$q_i = k\nabla^2 T \tag{3.1}$$

The metabolic heat generation (q_m) represents all tissue generated heat as a result of the aerobic and anaerobic metabolic processes. Energy storage regards to the amount of energy stored per unit mass of the tissue in consideration. When the rate of energy generated by tissues is different of the dissipation rate, the storage energy is changed and, consequently, changes in tissue temperature occur. The rate of change of stored thermal energy can be calculated by the following equation:

$$q_m = \rho c \frac{\partial T}{\partial t} \tag{3.2}$$

Finally, convection is the main type of heat transfer between tissues, occurring through the bloodstream by blood vessels. The contribution of blood vessels in the heat transfer process depends on their dimensional variety and on specific tissue irrigation, i.e., if the tissue is more or less irrigated. In this sense, the presence of blood vessels is crucial to the amount of heat that can be dissipated in tissues and, consequently, to the regulation of temperature. The convection mechanism (q_b) can be calculated through equation 3.3 [45, 45].

$$q_b = -w_b c_b (T_f - T_i) \tag{3.3}$$

where w_b and c_b represent the blood perfusion and blood specific heat, respectively, and T_f and T_i are the final and initial temperatures.

Hyperthermia ablation is a particular case of heat transfer where, in addition to the natural mechanisms of conduction, convection, metabolic heat generation, storage of thermal energy, energy from an external heat source also interferes in the generation, storage and absorption of metabolic heat. All these mechanisms can be combined in a single equation, called the Penne bio-heating equation 3.4 which allows the obtention of the resulting tissue temperature after exposure to electromagnetic radiation.

$$\nabla(-k\nabla T) = \rho_b w_b c_b (T_b - T) + Q_m + Q_s \tag{3.4}$$

where k represents the thermal conductivity of the tissue, ρ_b the blood density, c_b the specific heat of blood, w_b the blood perfusion, T_b the temperature of blood, and T the final temperature. Q_m and Q_s represent the metabolic energy source (metabolic heat) and the energy provided by the external source, i.e., the generated heat by the electromagnetic fields, respectively [30].

In this work, for a better approximation to what actually happens in the tissues, the value of effective thermal conductivity k_{eff} was considered, with respect to the specific value of the tissue thermal conductivity, considering the contribution of tissue blood perfusion [11, 43].

Several mathematical models have been developed based on this equation to describe the process of heat transfer within the biological tissues and to estimate the temperature and time values of exposure to electromagnetic radiation for the investigation and development of new electromagnetic radiation hyperthermia techniques. These models have been widely used for the analysis of local hyperthermia for cancer treatment [26, 44].

Most heat transfer problems in real situations involve complex geometries, are non-linear problems and their initial and boundary conditions lead to the use of numerical methods for their resolution. The most recurrent numerical methods to solve this type of problems are the finite element method (FEM) and the finite difference time domain method (FDTD). The FDTD method belongs to the class of numerical modeling methods based on the time differential domain, which is governed by the Yee algorithm and the time-dependent Maxwell equations whose discretization is done using approximations to space and time partial derivatives. FEM models are a simpler alternative, providing users with a tool for fast and accurate solutions to multiple systems of differential equations and, therefore, are well suitable for heat transfer, such as hyperthermia ablation [18, 26].

These approaches are the commonly used in simulation tools available for model building, numerical resolution, simulation, and post-processing of results, such as COMSOL Multiphysics, Sim4life, and Ansys.

3.2 Examples of Simulators of Tissues Heating by Electromagnetic Simulation

3.2.1 COMSOL Multiphysics

COMSOL Multiphysics is a simulation platform based on advanced numerical methods, such as the finite element method (FEM) and partial differential equations (PDE), for modeling and simulation of physics-based problems. COMSOL Multiphysics modules, such as AC/DC, MEMS, RF, chemical engineering, structural mechanics, earth science, electrochemistry, heat transfer, etc., provide additional interfaces for electrical, mechanical, fluidic and chemical applications. Beyond the physical modules and platforms for interaction with other software such as MATLAB, AutoCAD, SOLIDWORKS, etc., COMSOL Multiphysics has other modules, such as one of optimization, a material library and particle scanning, that make it a complete tool for solving physical problems [22].

COMSOL Multiphysics uses different numerical methods in the many additional modules which include finite element analysis, finite volume method, boundary element method and particle scan method, however, COMSOL Multiphysics emphasizes the FEM method. The COMSOL simulator provides several types of finite elements, being automatically generated by the program at the time of resolution. This patented finite element generation solution allows unlimited multiphysical combinations. Thus, several modules can be perfectly combined to deal with more consistent and precise applications when compared with reality [22].

Regarding the transfer of heat, COMSOL Multiphysics comprises a module that provides simulation tools to study mechanisms of heat transfer (radiation, convection and conduction) often associated with other physical phenomena such as fluid dynamics, electromagnetism, structural mechanics and chemical reactions. For this module, is essential the ability to perform calculations related to heat conservation or energy balances, where a variety of phenomena, such as mechanical losses, joule heating, etc., are available. This module provides a set of pre-fabricated physical interfaces, which are configured to receive the inputs from the models, from the user interfaces (GUI). As with all other interfaces of the COMSOL Multiphysics modules, is possible to manipulate the equations underlying the problem to provide greater flexibility allowing the user to modify transfer mechanisms, define a specific heat source or coupling different physical phenomena when necessary [22].

The heat transfer module provides a specific physical interface to Penne's bio-heating equation. The "bio equation" interface is the ideal tool to simulate thermal effects in human tissues or other biological systems, either by heating with electromagnetic radiation (microwave, RF, etc.), resistive heating, physical reaction heating or radiative heating. As always, in the COMSOL Multiphysics simulation environment, temperature changes can be easily modeled according to the properties of the materials, such as the electrical properties of the material. Bio-heating can be combined with a wide variety of phase change phenomena, such as tissue necrosis. In addition, through a series of different interfaces, COMSOL Multiphysics and the heat transfer module have the ability of processing possible interruptions created by a phase change, such as sudden changes in the electrical properties of the materials (electrical conductivity, thermal, etc.) or a change in flow behavior that may induce latent heat in the models. They also support the automatic definition of thermodynamic properties, and also include the ability to model changes in system volume through moving meshes [22].

3.2.2 COMSOL Multiphysics

ANSYS software offers a comprehensive set of tools for simulating and modeling problems related to any area of physics. ANSYS allows the development of products in the most wide-range engineering areas, such as electromagnetism, systems and structures, semiconductors and fluids, as well as the possibility of coupling physical problems (multiphysics) and an adaptive architecture that make this simulator efficient and innovative, once it allows to reduce physical constraints and to perform simulation tests for solving more or less complex problems that otherwise would not be possible [23].

The ANSYS electromagnetics module allows designing, simulating and validating the performance and operation of microwave and radio frequency (RF) antenna components. Integrated microwave and RF circuits and the modeling capabilities of this kind of systems are integrated into the ANSYS electromagnetic radiation solvers, providing a platform for verification of a complete microwave and RF system. The thermal management solutions of the ANSYS electronics modules promote advanced solution technology based on an automatic element mesh to enable a fast realization of heat transfer and simulation of fluid flow for cooling and convection strategies [23].

ANSYS has simulation modules for 3D products, such as ANSYS AIM. This offers a platform for the development of simulation-oriented products characterized by its versatility, speed and precision for project optimization. In addition, whether it is multiphysical couplings, thermal, electromagnetic, structural, fluidic, etc., AIM makes possible to solve problems without having to resort to any other simulation software for designers [23].

Fluid forces, thermal effects, structural integrity, and electromagnetic radiation are factors that can affect the performance of products and processes. In fact, these physical phenomena act at the same time and, in this sense, ANSYS has developed multiphysical solutions that can help the user to understand the effects of these phenomena (combined or isolated) to achieve a solution of great reliability and accuracy, when compared to the real world. The multiphysical solutions that ANSYS has developed include: electronic cooling, heat transfer, thermal analysis, etc. Regarding to heat transfer, ANSYS allows the simulation of heat transfer mechanisms such as convection, radiation (forced or natural) and conduction of heat in solids [23].

3.2.3 Sim4Life

The Sim4Life platform offers a wide-range of human computer phantoms, enabled with effective physics solvers and technically advanced biological tissue models, which provide a more realistic biological and anatomical environment for conducting fundamental mechanical studies, enable to test the effectiveness and safety of devices and medical treatments, and are a complementary tool to clinical trials, based on the Virtual Population ViP 3.0 models of the IT'IS foundation in Zurich [24].

Sim4Life integrates a parametric 3D modeling environment, which is based on the ACIS toolkit to development of advanced CAD models and high-quality tissue surface models. This is the only simulator capable of converting triangular surface meshes into parameterized CAD models and offers an integrated functionality to extract, smooth and simplify the surfaces of tissues and organs from segmented medical image data [24].

The comprehensive and versatile Sim4Life simulation platform includes a wide-range of specialized applications with optional modules such as Vagus nerve stimulation modeling, intentional and unintentional neuro-stimulation modeling by electromagnetic fields, thermal therapies, wireless energy transfer, etc. In addition to the software tools, each module includes a large set of models, own documentation and certified validation, as well as measurement tools [24].

Regarding to thermal therapies, Sim4Life allows modeling for device design as well as planning of specialized treatments. Electromagnetic radiation induced heating in both steady state and transient state can be simulated from the "P-Thermal" module. This is governed by Penne's bio-heating equation and considers sources of metabolic heat and electromagnetic energy, diffusion and heat transfer by tissue perfusion, with the possibility of considering local thermoregulation by vaporization, as well as the increase of temperature inside the body over time. Sim4Life provides a database of tissue properties that also includes thermal and perfusion parameters for a wide variety of tissues [24].

The "in vivo" induced effects can be predicted or evaluated through the thermal dose. A wide range of damaged tissue models is also available in Sim4Life (T-CEM43), such as the Arrhenius model that allows direct evaluation of tissue damage in coagulation zones and cell necrosis in ablation therapies. The thermal dose CEM43 expresses the thermal history of a tissue location in minutes of heating at 43 °C, which would result in an equivalent thermal effect [35].

The simulation of thermal therapies with Sim4Life is supported by a series of verification and validation tests. The electromagnetic and thermal solvers were systematically verified for correct implementation of the physical and numerical phenomena of the mathematical model underlying the problem. Dosimetry measurement settings with body phantoms and robotic scanning sensors have determined the correct modeling and performance of the power source (applicator). Thermal measurements were then performed through a variety of methods, such as thermometry or invasive or non-invasive measurements by a thermal catheter, in phantoms or patients. In addition, for matrix applicators, such as those used in deep hyperthermia or multiple catheter ablation treatment, the phases and amplitudes of the individual antennas are optimized to obtain optimal tumor coverage, avoiding tissue overexposure to radiation. In this sense, the Sim4Life also offers an automatic and rapid optimization of parameters for the hyperthermia treatment, allowing the definition of multiple treatment regions, as well as the weighting and reflection of the treatment priority and tissue sensitivity [24].

3.3 Conclusions

From the review previously presented, it is possible to realize that for understanding the phenomenon of tissue heating by electromagnetic radiation, is important to understand that the human organism itself has its own capacity to maintain body temperature constant. In this sense, by suffering temperature variations due to the application of external energy sources, the organism will trigger thermoregulation mechanisms that will counteract this variation which may affect the entire process of hyperthermia tumor ablation treatment. Furthermore, it is necessary to consider the different mechanisms of heat dissipation that can occur during its propagation along the tissues, since they are factors that will determine not only the final temperature that can be reached but also the time of exposure to which the patient can or must be submitted. Finally, all these factors can be combined in a single equation, called Penne's bio-heating equation, which allows the resulting temperature to be obtained after exposure to electromagnetic radiation.

The modeling and simulation of tissue heating for cancer treatment is a very current topic, in which has been perform several researches and developed numerous models. Most of these studies are governed by computational simulations based on advanced numerical methods, such as the finite element method (FEM) and finite difference method (FDTD). For this, there are several simulation tools that allow the construction of models, resolution by numerical methods, simulation and post-processing of results, such as COMSOL Multiphysics, Sim4life and Ansys.

Although these methods are a very efficient, fast and accurate tool that provides a means of calculation in the three-dimensional domain of electromagnetic fields and temperature, they do not allow the realization in a single environment of simulations that also include the electronic circuits of electromagnetic radiation generating systems. To bring the electromagnetic propagation and the heating of tissues to the domain of the electrical simulation, and thus to obtain a unique environment of simulation of the entire process, it is necessary to develop an equivalent electrical model that allows simulating the propagation and the effect of the electromagnetic radiation in biological tissues.

Chapter 4

An Electrical Model of Tissue Heating

4.1 Analysis of Electrical and Thermal Circuits

The analysis of thermal domain phenomena can be done using the same fundamental principles used in the analysis of electrical circuits. Kirchhoff's laws state that current flowing into a node (or junction) must be equal to the current flowing out of it (1st Law), and that the sum of all voltages around any closed loop in a circuit must equal zero (2nd Law). The same can be applied to thermal circuits if one replaces power with current and temperature with voltage. Both cases resistances hinder the flow of a quantity through the representing circuit (figure 4.1) [12].
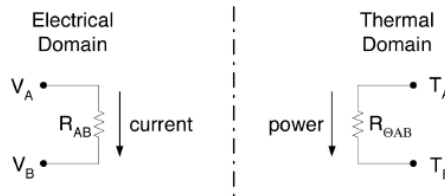
Figure 4.1: Fundamental relationships between both electrical and thermal domains [12].

In circuit theory, the resistance R_{elec} presented by an element is defined as the ratio of electric potential difference ΔV across that element, to the electric current I traveling through that element, according to Ohm's law,

$$R_{elec} = \frac{\Delta V}{I} \qquad (4.1)$$

Within the context of heat transfer, the respective analogues of electric potential and current are temperature difference ΔT and heat rate q, respectively. Thus, in the electrical equivalent of a "thermal circuit" thermal resistance R_{th} is given by

$$R_{th} = \frac{\Delta T}{q} \tag{4.2}$$

The duality between the two systems extends to both transient and steady-state conditions. The existence of capacities in both domains results in thermal RC time constant response, such as that found in the electrical domain. The thermal capacity is a function of the temperature increase associated with a certain amount of energy applied. The equation for thermal capacity C_{th} is:

$$C_{th} = \frac{q \cdot t}{\Delta T} \tag{4.3}$$

where q represents the transferred heat per second, t time (in seconds), and ΔT the variation of temperature (in $^\circ C$).

However, to avoid common mistakes, notice that there are two main differences between the two domains. First, in the electric domain the current is restricted to the flow through the specific elements of the circuit, while in the thermal domain, temperature is more diffuse, emitting from the source of radiation in three dimensions. On the other hand, coupling between elements is generally a more frequent behavior in the thermal domain. Usually, it is easier to use insulated devices in the electrical domain than in thermal networks. Thus, the development of good thermal models requires the use of coupling elements, unlike what happens in many electrical circuits [12].

Regarding to thermal circuits, the heat source feeds successive RC networks that model the behavior of the model to be simulated. The values of resistances R and capacitors C can be estimated through the physical properties and dimensions of the materials or can be extracted from empirical tests. For example, when a system is powered and is in steady state, thermal resistances can be calculated from the dissipated energy and temperature at the three thermal nodes ($T_{junction}$, T_{case}, $T_{hheatsink}$), (figure 4.2) [12].
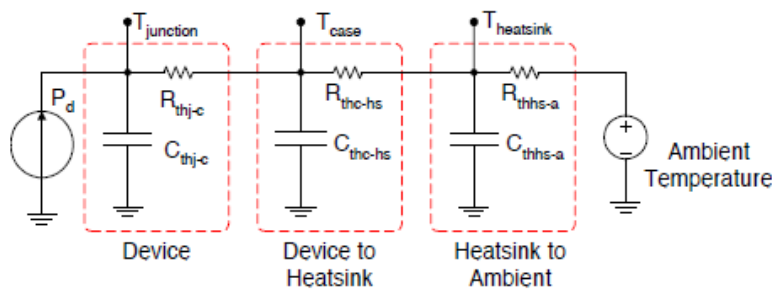
Figure 4.2: Example of a thermal circuit, adapted from [12].

Considering, for instance, the case of a planar wall (see figure 4.3) in which the main direction of heat flow occurs parallel to the x coordinate axis, thermal resistance may be obtained according to:

$$R_{x,con} = \frac{T_{s1} - T_{s2}}{q_x} = \frac{L}{\lambda A} \tag{4.4}$$

where, L is the length through which heat (q_x) flows, A is the transverse area, and λ the wall conduction coefficient.
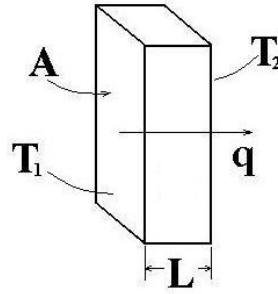
Figure 4.3: Illustration of Fourier's law of conduction, adapted from [13].

Fourier's law of conduction relates heat rate (q) (in W) within a linear medium of conduction coefficient λ, cross-sectional area A, and temperature distribution $T(r)$, to the temperature gradient as follows:

$$q = -\lambda A \nabla T \tag{4.5}$$

Newton's law of cooling relates the one-dimension convective the flow (along dimension x) q_x from surface to the difference between surface and ambient fluid temperatures (T_s and T_∞, respectively) through a proportionality constant h, as follows:

$$q_x = hA \left(T_S - T_\infty \right) \tag{4.6}$$

The proportionality constant h depends on a variety of parameters governing a specific flow condition (fluid density, viscosity, speed, turbulence, etc.). The subscript on T_∞ indicates its reference to fluid temperature at distances far from near-surface boundary-layer temperature variations. Each of these laws may be expressed as heat flux, $q'' = q/A$.

In the transient state, the characterization of the system response requires the monitoring of the temperature response at a given input power [12].

In thermal circuits, since ground is a node within the thermal domain, it must represent some reference value of temperature. Thus, there are two choices for this reference temperature value: ambient temperature or absolute zero. In addition, as shown in the illustration of figure 4.2, the capacitor is connected to a reference terminal. However, a circuit having an equivalent thermal

response can be created so that each capacitor is connected in parallel with the thermal resistances. Any of these assemblies is valid, assuming that the component elements are replicated to each node [12].

4.2 Characterization of the Dielectric and Thermal Properties of the Biological Tissues

4.2.1 Dielectric Properties of Biological Tissues

From what was mentioned before, it is possible to understand that the interactions between EM fields and tissues are determined by their dielectric properties and that these are frequency dependent. In this sense, it is important to know the values of the dielectric properties of tissues, considering their variability with frequency, to perform a more reliable electrical simulation of the EM propagation through biological tissues [46].

To better understand how human tissues are characterized, their dielectric properties were analyzed together from some of the available literature. Since this work is intended for the electrical simulation of the hyperthermia treatment for breast tumors, all the presented data is relative to the human breast tissue. Regarding to the classification of the breast tissue, in this work the following layers of biological tissues were considered: skin, fat, gland and cancerous tissue. Furthermore, it should be noted that the presented data is a result of data extrapolation obtained from the graphics and tables of the different authors, so it is not necessarily precise [47, 48].

C. Gabriel et al. used a technique based on an automatic swept-frequency network and in an impedance analyzer to measure the dielectric properties of human tissues such as fat and skin, in the frequency range from 10 MHz to 20 GHz at 37 °C. Furthermore, they developed a parametric model to describe the variation of the dielectric properties of tissues with frequency in the range from 10 Hz to 100 GHz at 37 °C [46, 49]. J. Andrzej et al. measured the relative permittivity of breast carcinoma and the surrounding tissues including fat and normal breast tissue. The experimental procedure was performed in frequencies between 20 kHz and 100 MHz at 37 °C [50]. W.T. Joines et al. used a flat-ended coaxial probe connected to a network analyzer to measure the electrical conductivity and relative permittivity of malignant and normal human tissues, including the breast gland, in a frequency range from 50 MHz to 900 MHz between 23 °C and 25 °C [51]. In this study, the dielectric properties were obtained from Andreuccetti et al. which in turn was based on the parametric model developed by C. Gabriel et al. to develop an online application aimed to calculate the dielectric properties of human tissues in a frequency range between 10 Hz and 100 GHz. With the aim of including the ISM frequencies for medical purposes, the range of frequencies chosen in this work is from 10 MHz and 2.5 GHz. In this sense, the considered values of permittivity and conductivity of each tissue for the different frequencies used are shown in table 4.1 [30, 16].

Table 4.1: Dielectric properties of each tissue for the different frequencies used in the simulated models [16].

	Skin		**Fat**		**Gland**		**Tumor**	
Frequency (MHz)	ε_r	σ	ε_r	σ	ε_r	σ	ε_r	σ
13.56	285.25	0.238	7.1794	0.0283	132.35	0.7294	290	0.79
27.12	165.03	0.3289	6.2656	0.0288	93.908	0.7508	190	0.82
433	46.079	0.7019	5.5075	0.0352	61.332	0.886	57.9	0.89
915	41.329	0.8717	5.4219	0.0495	59.65	1.0444	57.1	1.16
2000	38.568	1.2654	5.2323	0.1061	57.85	1.6333	56	1.8

The extrapolated data collected from the different researchers and the values considered in the current study for the different tissues in the frequency range of interest are presented in a graphical form, figure 4.4 and figure 4.5.

From the analysis of this data, it is possible to verify that there exists some inconsistency in the values. However, there are possible reasons that can justify this variability. First, the extrapolation made from the other graphs to deduce a value for a specific frequency value can lead to large uncertainties compared to the real value. Secondly, the characterization of breast tissue in the literature is ambiguous, i.e., the composition of normal breast tissue can vary depending on the tissue layers being considered. For example, some researchers divide the breast tissue in three types of tissues: fat, connective and glandular, and others may even consider the fibrous tissue, muscle, etc. In addition, regarding to the malignant tissues, the different stages of tumor development will change its dielectric properties. Moreover, the measurements are performed on different patients, what can introduce a large variability since the water and fat content may be different from person to person. Furthermore, if the patient is in stage of menstruation, breastfeeding or pregnancy the values of dielectric properties of tissues can also vary [48].

Despite of the values inconsistency, it is possible to observe that in all researches, including in the current study, the malignant tissues have higher permittivity and conductivity than the normal breast tissues. Furthermore, the fat tissues have the lowest permittivity and conductivity so, regarding to this, it is reliable to consider the values calculated from [43] for the different simulated models in this work [48].

4.2.2 Thermal Properties of Biological Tissues

Similarly, for the construction of a thermal model of biological tissues heating it is important to know its thermal characteristics. In this sense, for the thermal characterization of the biological tissues, data from some of the available literature were analyzed together. M.P. Robinson et al. used differential scanning calorimetry to measure the heat capacities and density of some human tissues such as breast fat at a body temperature of 37 °C [52]. H.F. Bowman used a thermal diffusion probe to measure the in vitro "intrinsic" thermal conductivity of human tissues including skin, fat, normal breast and breast carcinoma at 37 °C [53]. M. Gautherie used a thermoelectric
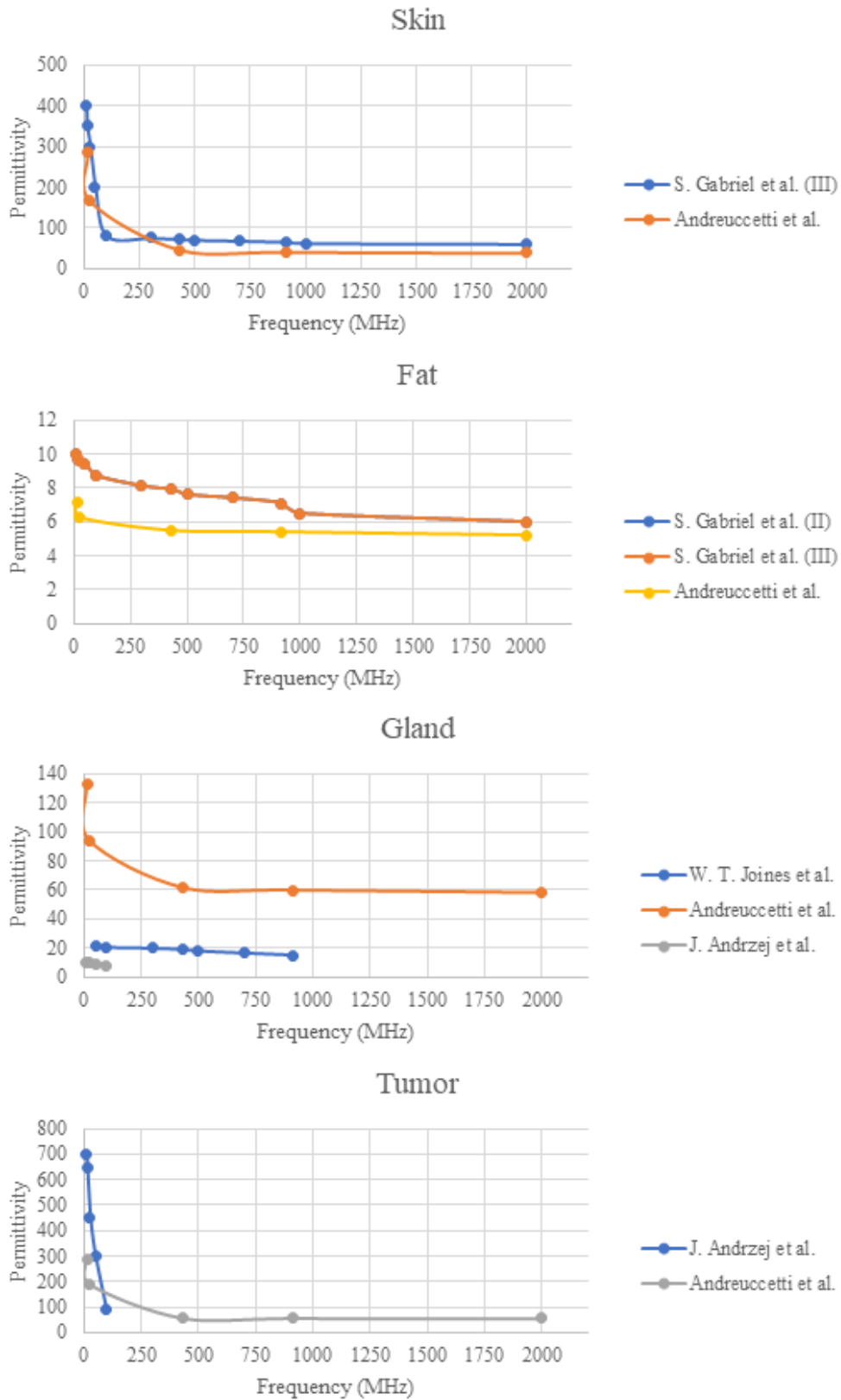
Figure 4.4: Permittivity of tissues: Skin; Fat; Gland; Tumor.
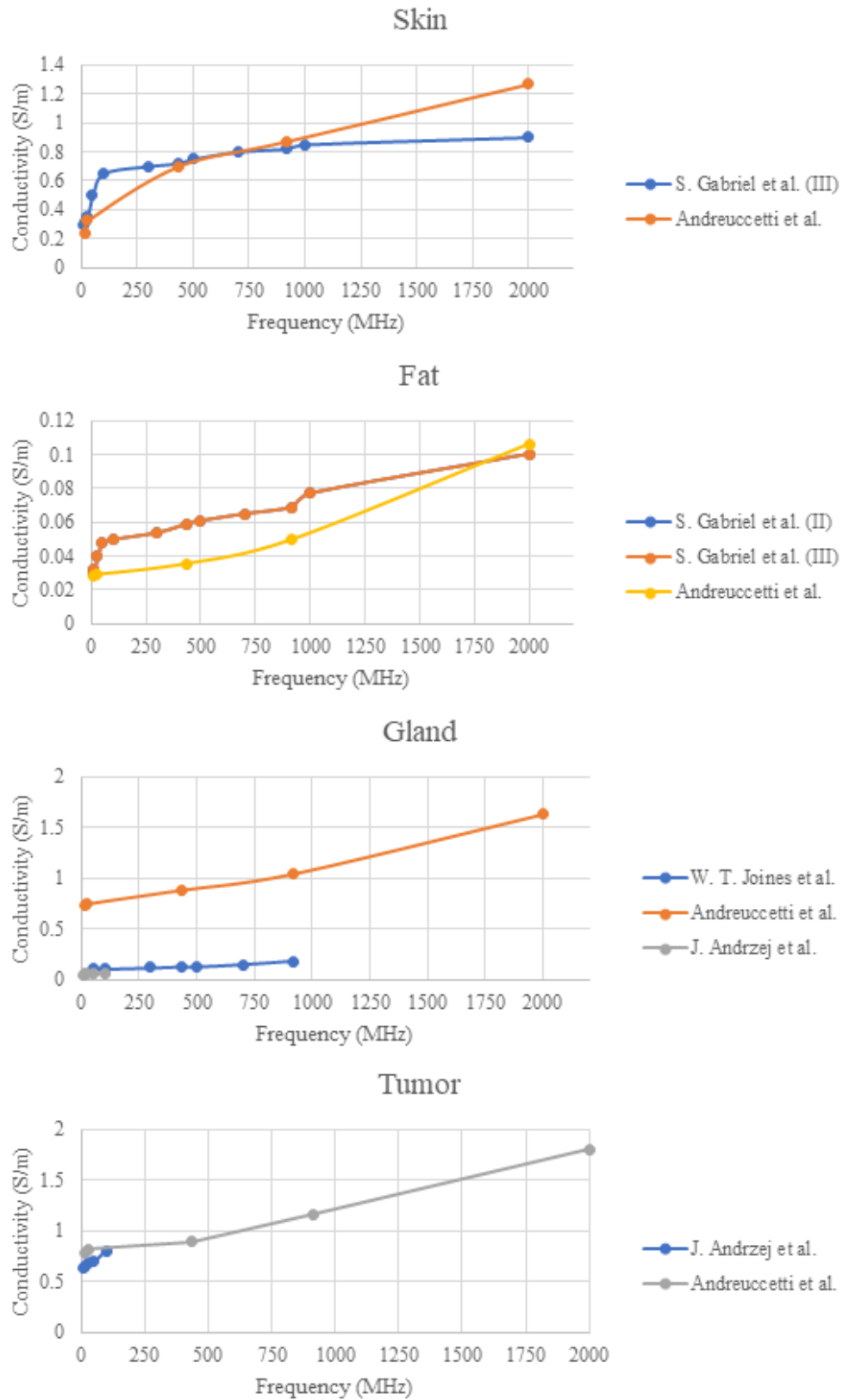
Figure 4.5: Conductivity (in S/m) of tissues: Skin; Fat; Gland; Tumor.

fine-needle to perform a series of measurements of the effective thermal conductivity of normal and malignant breast tissues. Tissues types include fat, fibrous or glandular depending on the mammary structure of patients [54]. F.J. González performed thermal simulations based on the finite element method of a simplified model of a female breast to quantify the minimum tumor size to be detected in a localized infrared imaging system where both normal and cancerous tissue were considered to have a thermal capacity, density and effective thermal conductivity of 3000 J/Kg°C, 920 Kg/m^3 and 0.42 W/m, respectively [55]. P.A. Hasgall et al. developed a database of tissue properties that provide values for EM, thermal, fluid, acoustic and MR properties of biological tissues. Tissues types include breast fat, breast gland and skin [56].

The extrapolated data collected from the different researchers for the different tissues are presented in table 4.2.

Table 4.2: Thermal properties obtained from data collected in the literature.

Tissue	k	C	ρ	Reference
Fat	-	2.22	93400	[M. P. Robinson et al.]
Breast	0.499	-	-	[H. F. Bowman]
Fat	0.219	-	-	
Skin	0.498	-	-	
Tumor	0.397	-	-	
Fat	0.171	-	-	[M. Gautherie]
Gland	0.37	-	-	
Tumor	0.511	-	-	
Normal Breast	0.42	3	92000	[F. J. Gonzalez]
Malignant Breast	0.42	3	92000	
Skin	0.37	3.391	1109000	[P.A. Hasgall et al.]
Fat	0.21	2.348	911000	
Breast Gland	0.33	2.96	1041000	

From the analysis of this data it is possible to verify that there exists a slight inconsistency in the values. Although the variability of values is much smaller when compared to those obtained for the dielectric tissues characterization, the explanation of this phenomena can be explained through the same factors.

To guarantee a better approximation of the model to the reality, a boundary condition on the skin surface was considered, which includes the heat transfer due to convection, radiation and evaporation from the skin to the surrounding environment. In this sense, the heat resistance was determined, considering a total heat transfer coefficient (U) of 13.5 W/m^2°C, according to equation 4.7, and set to 2962.96 °C/W on the thermal model [57, 58].

$$R_{heat} = \frac{1}{U} \qquad\qquad (4.7)$$

4.3   An Equivalent Electrical RC Model of Biological Tissues

Biological material is composed of cells in an ionic extracellular medium. Cells can be seen as a characteristic insulating membrane, called cytoplasmic membrane, which involves the intracellular environment (cytoplasm) made of several ions. Electrically, the cytoplasm can be modelled as a conductive medium, due to the presence of a large ion concentration, being characterized by a specific value of conductivity, σ [48, 59].

Outside the cell there is more fluid, the extracellular fluid, comprising several types of ions, that can be modelled as a conducting medium with a specific value of conductivity. On the other hand, the cytoplasmic membrane is relatively isolating, giving the cell specific dielectric properties. The membrane is a thin layer of selective permeability that can be modelled as a capacitive medium with a certain relative permittivity value associated, ε_r [59].

Tissues are groups of cells surrounded by conductive extracellular fluid. In some regions, the cells are extremely attached to each other so, any current flowing can pass through the membranes. On the other hand, other zones constitute gaps, through which current cannot pass. Although the detailed modelling of cells and gaps is a very complex process, it is possible to obtain reasonable approximations of tissues' electrical equivalent circuits. Thus, with a simple RC electric circuit it is possible to model the changes in resistivity and electrical capacity of tissues with frequency [59, 60].

In this sense, according to the circuit shown in figure 4.6, resistance R represents the resistivity of the electric paths through the extracellular and intracellular fluids that model the resistive cells' behavior, whereas the capacitor C models the capacitive characteristics of cell membrane [48].
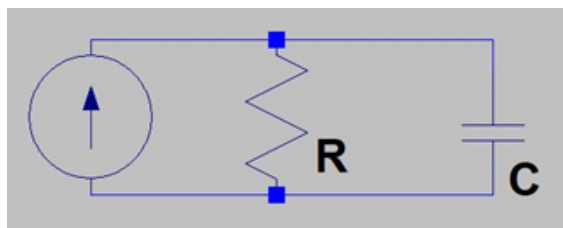
Figure 4.6: Representation of the equivalent RC model of each tissue, drawn in LTspice IV.

Starting from the specific case of using RC circuits for modelling human tissues represented by the illustration in figure 4.6, in this work the different tissue layers are considered with the minimal dimensions of a cube of 5 mm, each one represented by its specific RC circuit. Thus, for each cube of tissue it is necessary to first, determinate the initial incident power and then, knowing the penetration depth through biological tissues, calculate the power at a certain depth, and in turn calculate the temperature rise in the tissue [30].

Knowing that the power P dissipated in an electrical resistance R is given by $P = V^2/R$, for a capacitor C containing a dielectric material the power can be determined through the equation 4.8.

$$P = 2\pi f C_0 \varepsilon'' V^2 \tag{4.8}$$

For a parallel plate capacitor, the capacitance of free space C_0 is given by equation 4.9:

$$C_0 = \frac{\varepsilon_0 A}{d} \tag{4.9}$$

where A represents the plate area, d is the separation between plates and ε_0 is the permittivity of free space. In addition, voltage V can be determined by $V = E \cdot d$ and thus, power can be calculated according to equation 4.10.

$$P = 2\pi f E^2 \varepsilon_0 \varepsilon'' A \cdot d \tag{4.10}$$

Since $(A \cdot d)$ represents the tissue elementary volume, the power dissipated per unit of volume or power density is given by:

$$Q = 2\pi f \varepsilon_0 \varepsilon'' E^2 \tag{4.11}$$

Furthermore, as was mentioned before, as the electromagnetic energy penetrates through the material, it attenuates to an extent depending on the attenuation constant or skin depth. In this sense, the power dissipated per unit volume exponentially decays as the energy traverses across the dielectric material, according to the following equation:

$$P = P_0 \cdot e^{-2x/\delta} \tag{4.12}$$

where P_0 is the incident power and δ the penetration depth. Thus, after the determination of the power dissipated in the target tissue by equation 4.12, and knowing the heating time (t), it is possible to calculate the variation of temperature that occurs during the heating process by the following equation 4.13:

$$\Delta T = \frac{t \cdot P_t}{c \cdot \rho} \tag{4.13}$$

where c represents the specific heat, ρ the density, and P_t the power in the target tissue [30, 3, 61].

4.4 Electrical Model of the Propagation of Electromagnetic Radiation Through Biological Tissues

4.4.1 One Spatial Dimensional Equivalent Electrical Model of the Propagation of the Electromagnetic Radiation Through Tissues

From the specific case of an elementary RC equivalent electrical model a linear electrical model was developed. This consists of a series of tissue's blocks representing each layer of breast tissue. As mentioned before, each type of tissue includes skin, fat, breast gland and tumor. Each block of tissue represents an elementary cube with edges 5 mm long, as shown in figure 4.7.
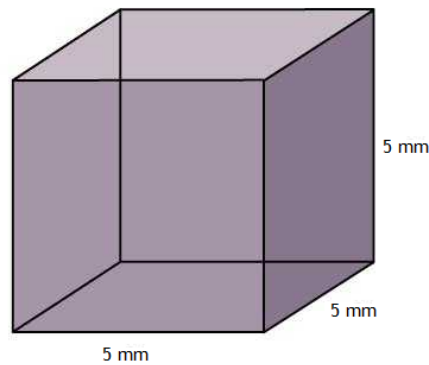
Figure 4.7: Illustration of a tissue elementary cube with edges 5 mm long [14].

In the model, each impedance constituted by an electrical resistance R and a capacitor C represents a 5x5x5 mm^3 volume of tissue layer, the power supply represents the radiation emitted from an antenna that hits the skin surface, and the connections among elementary cubes represent the EM propagation through tissues. Besides, for representing the transmission of EM radiation through air it was considered an impedance of free space of 377 Ω. A representation of the impedance developed for representing each tissue layer and an illustration of the model constructed in ADS Software are shown in figure 4.8.

To perform simulations to study the contribution of the rest of the body, the previously described model was rearranged. A new component was constructed now with the associations of the surrounding tissues. The illustration of the model developed in ADS Software is represented in figure 4.9.

For the electrical characterization of tissues, the electrical resistance (in Ω) and capacitance (in F) were calculated, respectively, using the equations 4.14 and 4.15.

$$R = \frac{1}{\sigma}\frac{l}{A} \qquad\qquad (4.14)$$
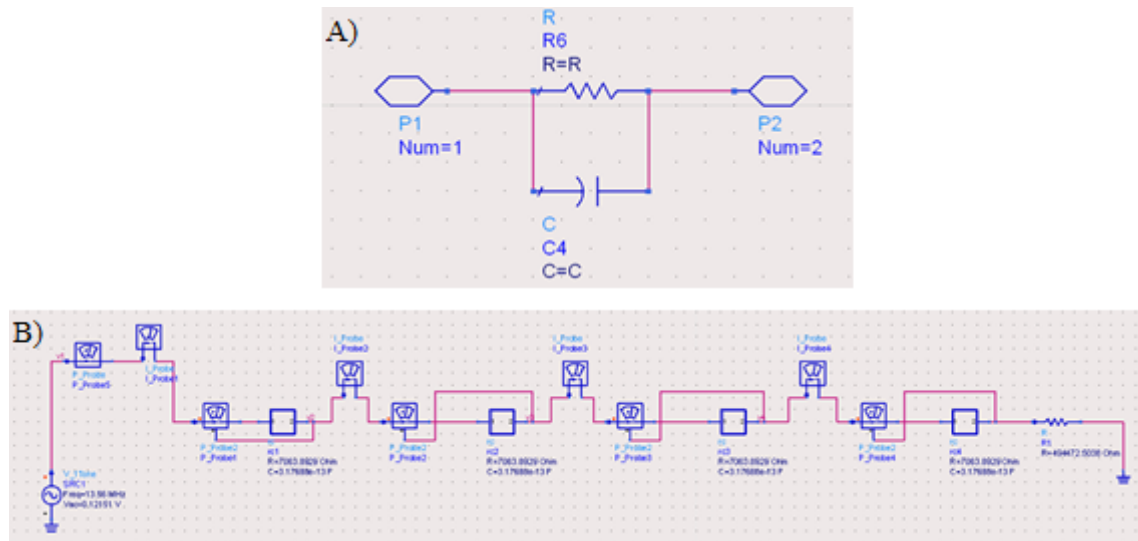
Figure 4.8: (A) Representation of the impedance developed for representing each tissue layer; (B) linear model of tissues developed in the ADS.
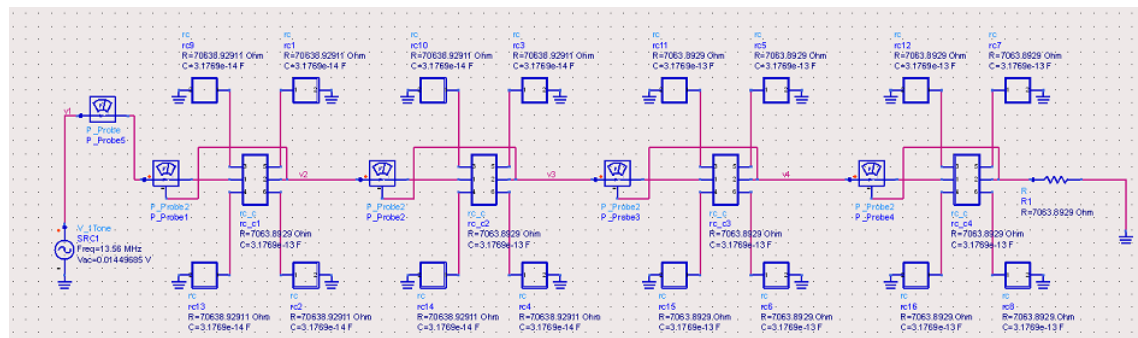
Figure 4.9: Linear model of biological tissues with the associated contribution of the body developed in the ADS.

$$C = \varepsilon_0 \varepsilon' \frac{A}{l} \tag{4.15}$$

where σ represents the tissue conductivity, l the thickness and A the tissue area, for the electrical resistance. Regarding to the capacitance, ε_0 represents the vacuum permittivity and ε_r the relative permittivity of tissue. The obtained results of each tissue type for the different frequencies are presented in the tables 4.3 and 4.4.

Table 4.3: Resistance (in Ω) of each tissue used in the simulated models.

Frequency (MHz)	Skin	Fat	Gland	Tumor
13.56	840.266	7063.893	274.217	253.165
27.12	608.143	6936.496	266.386	243.90
433	284.941	5674.886	225.726	235.294
915	229.439	4038.5276	191.498	172.414
2000	158.053	1884.659	122.451	166.667

Table 4.4: Capacitance (in F) of each tissue used in the simulated models.

Frequency (MHz)	Skin	Fat	Gland	Tumor
13.56	1.262e-11	3.177e-13	5.856e-12	1.106e-11
27.12	7.3e-12	2.77e-13	4.16e-12	8.41e-12
433	2.039e-12	2.437e-13	2.714e-12	2.562e-12
915	1.829e-12	2.399e-13	2.64e-12	2.528e-12
2000	1.706e-12	2.315e-13	2.559e-12	2.478e-12

4.4.2 Transposition of the Equivalent Linear Electrical Model of Tissues to Three Dimensions

The developed model allows simulating the propagation of EM radiation through tissues and the surrounding environment at one spatial dimension. However, as it is well known, the propagation of the radiation occurs in three dimensions, per whole volume of tissue. In this sense, an optimization of the linear model for three dimensions was made.

The new 3-D model consists of a network of elementary 5 mm edge along cubes of tissues connected to each other along the three axes. For a better understanding of what was built in ADS software, an illustration of a cube modelling the different elementary cubes representing each layer of breast tissue is presented in figure 4.10.
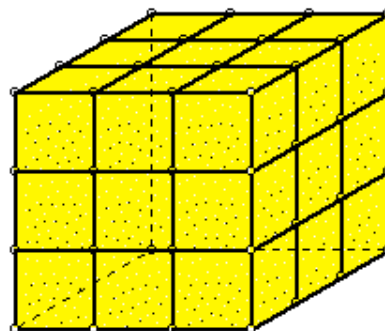
Figure 4.10: Illustration of the model considered, where each elementary cube represents a block of tissue corresponding to a certain type of breast tissue (skin, fat, gland or tumor) [15].

In this model, a component constituted by six RC circuits representing each elementary cube

face was built to model the power dissipated in each direction. Here, also the contributions of the surrounding tissues and the environment were considered. The illustration of the model developed in the ADS software is shown in figure 4.11.
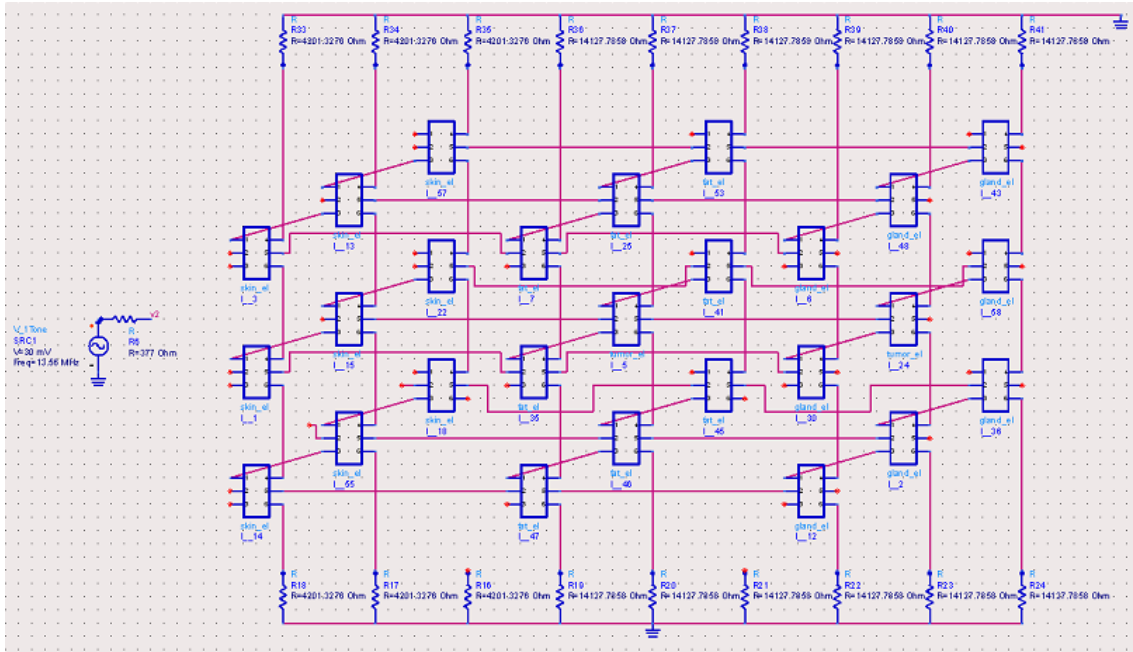
Figure 4.11: Representation of the 3-D electrical circuit model used in ADS.

4.5   Thermal Modelling the Heating of Biological Tissues

The development of an equivalent electrical model of the biological tissues not only allows studying the propagation of the electromagnetic radiation through tissues, but also to study the temperature variation over time, knowing the power dissipated in each elementary volume.

For this purpose, a component, named power sensor, was developed that allows converting the power dissipated in the electrical model into a current source, which in turn allows interconnecting the electrical model to the thermal circuit that models the heating of tissues. This block is composed by an SDD2P2 component that performs the calculation of the power dissipated after the current, that is measured by current probe (I_Probe) and the input voltage. A half-wave rectifier is connected at the terminals of the SDD2P component that allows the converting the obtained AC signal into a DC signal. A current-controlled current source is connected at the terminals of the rectifier to convert the power dissipated into a current, which in turn becomes the heat source connected to the thermal model of the target tissue. The schematic of the power sensor is presented in figure 4.12. Afterwards, a component including the six RC circuits representing each elementary cube face and the power sensor was built for the electrical model as shown in figure 4.13 [62].

For the thermal model, a component where the current source is connected to the center of the block modelled with six RC circuits used. Each block of tissue is connected to the neighboring
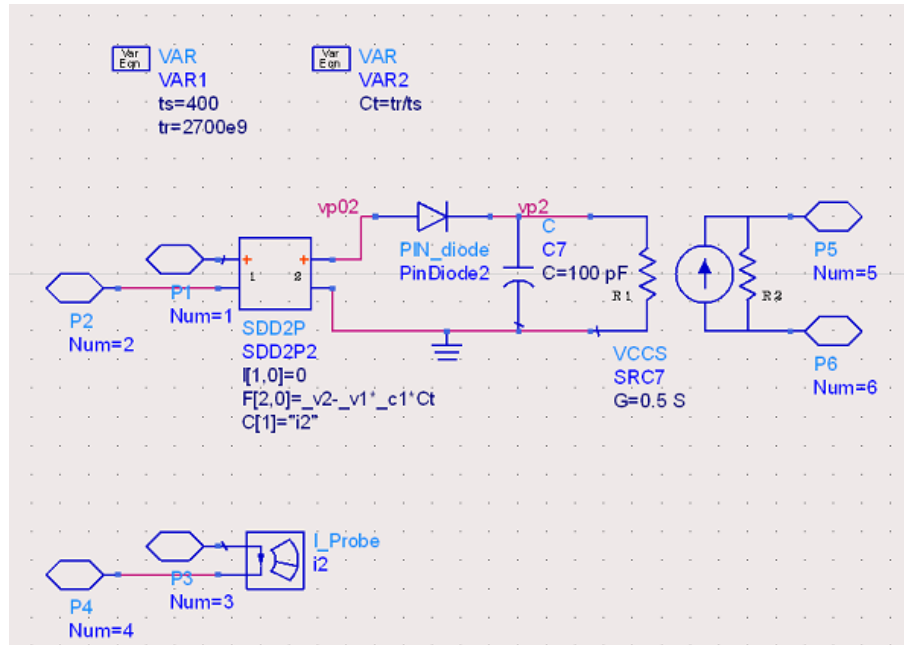
Figure 4.12: Representation of the power sensor developed in ADS.
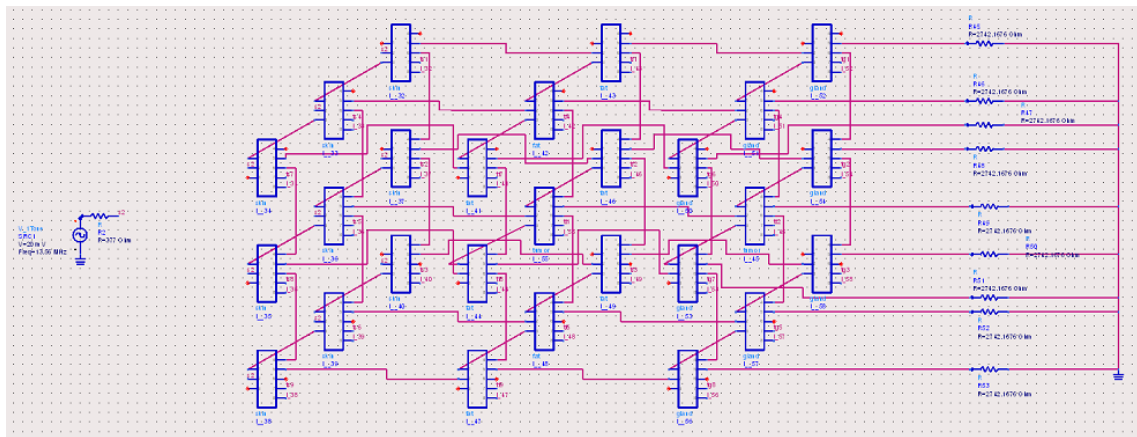
Figure 4.13: Representation of the 3-D electrical circuit model used in ADS.

ones in the different directions. In the thermal model, also the influence of the surrounding tissues and the environment were considered. As mentioned before, to represent the heat dissipation from skin surface to air, a thermal heat resistance was considered, and the reference temperatures were set to 25 °C and 37 °C for air and body tissues, respectively. The model developed in the ADS Software for the study of temperature variations in tissues over time is presented in figure 4.14.

The specific values of thermal resistance R_{th} (in °C/W) and thermal capacity C_{th} (in J/°C) representing resistance R and capacitor C of the RC equivalent circuits were calculated, respectively, using the equations 4.16 and 4.17.
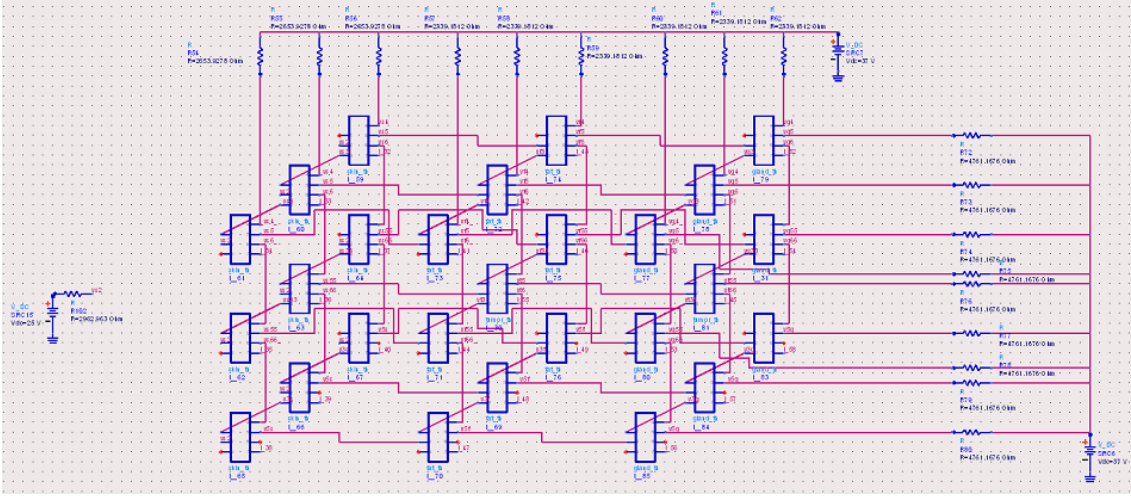
Figure 4.14: Representation of the 3-D electrical circuit model used in ADS.

$$R_{th} = \frac{l}{k \cdot A} \tag{4.16}$$

$$C_{th} = V \cdot c \cdot \rho \tag{4.17}$$

where l represents the tissue thickness, k the thermal conductivity, and A the section area, for the thermal resistance. Regarding to the thermal capacity, V represents the volume, c the specific heat and ρ the density of the tissue. The values that characterize the thermal properties of the different tissues are presented in table 4.5.

Table 4.5: Thermal properties of each tissue used in the simulated model.

	Skin	**Fat**	**Gland**	**Tumor**
Thermal Resistance (°C/W)	530.7856	1169.5906	476.1905	476.1305
Thermal capacity (J/°C)	0.4701	0.2674	0.345	0.345

4.6   Conclusions

From the review presented in this chapter, it is possible to understand that to perform the simulations of the thermal behavior of tissues submitted to EM radiation making use of the equivalent electrical circuits, it is important to have notion of the duality that exists between the two, electrical and thermal, domains. First, each domain comprises a variable that forces a floe, electric

current or heat flow. Secondly, both are defined by a source that generates a potential difference, which in the thermal domain is a difference of temperatures ΔT, and in the electric domain a voltage drops V. In addition, both systems have impedances that constrain the passage of flow through the circuit. Also, the existence of capacities in the thermal model give rise to a thermal RC time constant, similar to that of the electric domain, being that the thermal capacity is a function of the temperature increase associated with a determined amount of applied energy.

An equivalent electrical model of the tissues was developed, consisting of an association of elementary cubes, representing the different layers of tissues such as skin, fat tissue, breast gland tissue and tumor. With this model it is possible to simulate the heating of the tissues over time. However, this model only allows the user to have a one spatial dimension perception of the process, which does not correspond to what actually happens, since the propagation and dissipation of the electromagnetic radiation through the tissues occurs in several directions.

A more realistic perception of the heating process can be obtained a 3-D model that provides a better understanding of how the propagation of the radiation actually occurs in the different directions, as well as a better perception of how the distribution of heat occurs in the biological tissues.

Chapter 5

Tissue Heating Simulation and Results

5.1 Validation of the Linear Equivalent Electrical Model of Biological Tissues

5.1.1 Comparison of ADS Simulations with Theoretical Results

Regarding to the linear equivalent electrical model of tissues, first, it was calculated for 13.56 MHz and to 2 GHz at 0.01 V the incident power P_0 (in W) in fat tissue, according to the equation 4.10. As mentioned before, it is known that the power at a certain depth (in m) within the tissue is given by equation 4.12. Furthermore, knowing the incident power and the P(x), the power dissipated P_d (in W) in each block of tissue is calculated, according to equation 5.1.

$$Pd_i = P(x_{i-1}) - P(x_i), \qquad (5.1)$$

where P_d represents the power dissipated in a block of tissue at depth x.

For simulations in ADS, it was considered the linear model of biological tissues, as previously described, where each block of tissue was characterized as fat. The simulations were performed for the same value of frequency, and incident power obtained from theoretical equation. The results are presented in table 5.1 and illustrated in figure 5.1.

Table 5.1: Results for P(x) and P_d obtained from ADS simulations and equation 4.12, at 13.56 MHz.

Depth [m]	P(x) ADS Values [W]	P_d ADS Values [W]	P(x) Theoretical Values [W]	P_d Theoretical Values [W]
0	1.4150e-8	-	1.415e-8	-
0.005	1.3965e-8	1.848e-10	1.398e-8	1.731e-10
0.010	1.3780e-8	1.848e-10	1.381e-8	1.710e-10
0.015	1.3596e-8	1.848e-10	1.364e-8	1.689e-10
0.020	1.3411e-8	1.848e-10	1.347e-8	1.669e-10
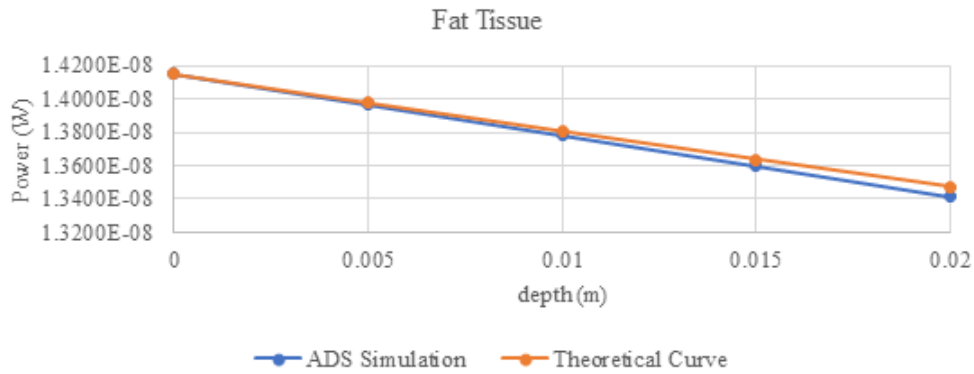
Figure 5.1: Power dissipated at a certain depth in fat tissue, at 13.56 MHz for ADS simulation and theoretical curve.

By the analysis of the graphic it is possible to observe that the ADS simulation result is very close to the theoretical curve, i.e., the behavior of both curves is similar since the power decreases as the penetration increases. However, it would be expected to see an exponential behavior as the EM energy propagates through the lossy material, as previously mentioned. Besides, it is possible to verify that the values of P_d are not the same along the x-axis, indicating the non-linear behavior of the equation 4.12.

From the ADS simulation, once only fat tissue was considered without the influence of the surrounding tissues, the dissipated power is the same along the x-axis, fact that can explain the linear behavior. However, regarding to the theoretical curve, the reason that may be influencing this result is the fact that, once the exponential behavior depends on the penetration depth, and for fat tissue at 13.56 MHz the penetration depth is 0.81 m, the power dissipated between the different penetrations is slight. Also, considering a depth smaller than the one compared to the skin depth may indicate that these values of incident power and depth cannot be enough to verify the exponential behavior. This lead to an approximation of a small region of the predicted theoretical curve corresponding, approximately, to a linear area, where the dissipated power is minor.

To assure that this is a possible explanation for the theoretical result, it was performed the same study but for a frequency of 2 GHz with a penetration depth of 0.03 m. The results are presented in table 5.2 and illustrated in the figure 5.2.

Table 5.2: Results for P(x) and P_d obtained from ADS simulations and equation 4.12, at 2 GHz.

| Depth [m]	P(x) ADS Values [W]	P_d ADS Values [W]	P(x) Theoretical Values [W]	P_d Theoretical Values [W]
0	5.304e-8	-	1.4150e-8	-
0.005	5.264e-8	4.004e-10	1.3977e-8	1.333e-8
0.010	5.224e-8	4.004e-10	1.3806e-8	9.980e-9
0.015	5.184e-8	4.004e-10	1.3637e-8	7.471e-9
0.020	5.144e-8	4.004e-10	1.3470e-8	5.594e-9
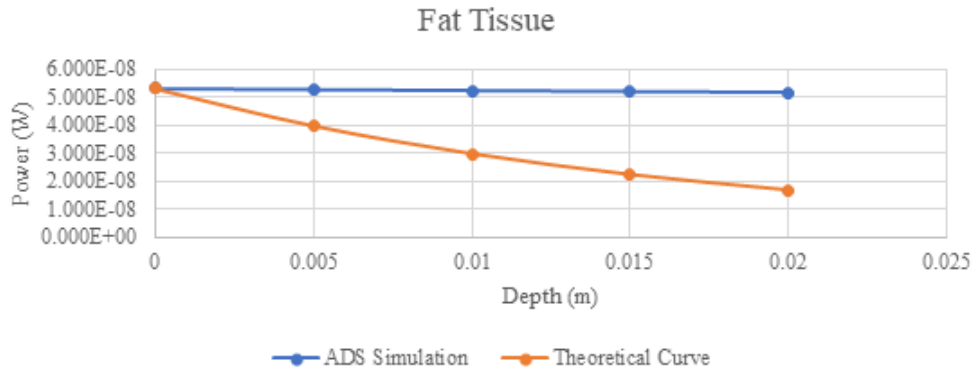
Figure 5.2: Power dissipated at a certain depth in fat tissue, at 2 GHz for ADS simulation and theoretical curve.

From the analysis of figure 5.2, it is possible to verify that once the skin depth is closer to the considered depth, the exponential behavior becomes clearer. Despite the power decrease with depth in both curves, as it was expected, since for the ADS simulation it was considered the linear model of fat tissue only, the P_d is the same as the EM energy propagates through the different blocks leading to a linear behavior along x-axis.

In this sense, for a better approximation of the model of what is expected, simulations for the linear model plus the contribution of the surrounding tissues were performed for 13.56 MHz and 2 GHz. In ADS software, the linear equivalent model for tissue plus body contributions was defined as 4 blocks with 5mm of fat tissue, each one with a different body contribution associated. The results of ADS simulation at 13.56 MHz and 2 GHz for $P(x)$ and P_d are presented in table 5.3 and illustrated in figure 5.3.

Table 5.3: Results for P(x) and P_d obtained from ADS simulations.

Depth [m]	P(x) Values for 13.56 MHz [W]	P_d Values for 13.56 MHz [W]	P(x) Values for 2 GHz [W]	P_d Values for 2 GHz [W]
0	1.415e-8	-	5.304e-8	-
0.005	6.160e-9	7.990e-9	2.380e-8	2.924e-8
0.010	3.113e-9	3.047e-9	1.238e-8	1.142e-8
0.015	2.764e-9	3.489e-10	1.108e-8	1.304e-9
0.020	2.758e-9	6.584e-12	1.105e-8	2.470e-11

From the analysis of the graphic, it is possible to observe that once the contribution of the surrounding tissues is considered, the response of the model is closer to what was expected, according to the theoretical equation based on the power dissipation within a lossy medium, such as the biological tissues. Besides, it is possible to verify that for the same values of depth, the power dissipated is higher for 2 GHz than 13.56 MHz.
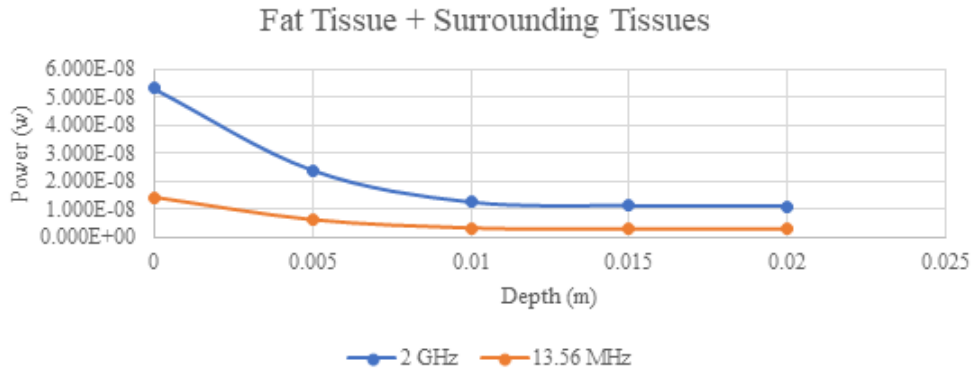
Figure 5.3: Power dissipated at a certain depth in fat tissue considering also the surrounding tissues is considered influence, at 2 GHz and 13.56 MHz for ADS Simulation.

5.1.2 Comparison of ADS Simulations with MATLAB Simulations

According to K. Emmanuel, the 1-D case of Penne's bioheat transfer equation is a good approximation of what happens in tissues when heat mainly propagates in a perpendicular direction to the skin surface. Thus, to validate the presented developed model not only of what concerns to the EM propagation but also to heat transfer, simulations were performed in MATLAB of an existing function of Penne's bioheat equation, at one dimension, see appendix A [63].

In this sense, the linear equivalent model of fat tissue was adapted, and a power sensor was included to measure the temperature T (in °C), in the linear thermal model, after a time t (in seconds) at a certain voltage (in V), as shown in figure 5.4. The simulations in ADS were performed at 13.56 MHz for 0.01 V, 0.1 V and 0.5 V, during 1200 s (20 minutes).
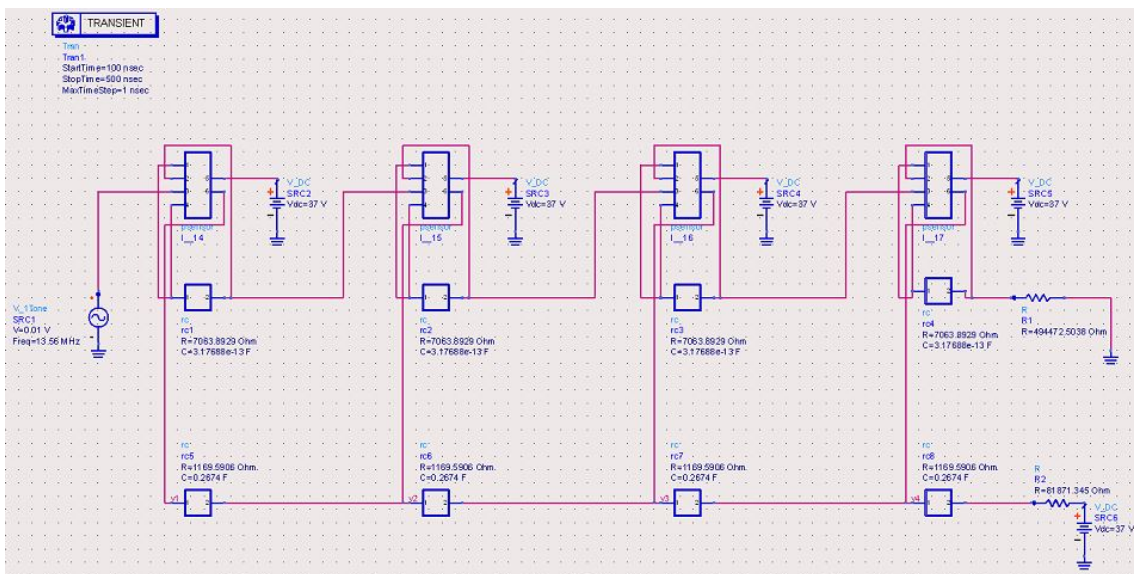
Figure 5.4: Representation of the linear model including the thermal model.

The simulations in ADS were performed at 13.56 MHz for 0.01 V, 0.1 V and 0.5 V, corresponding to an incident power of 9.583e-11 W, 9.853e-9 W and 2.396e-7 W, respectively, during 1200 s (20 minutes).

According to [12], thermal capacity is given by the temperature increase associated to a certain amount of energy applied. In this sense, knowing the variation of temperature in each block of tissue, tissue thermal capacity and time, it is possible to determinate with equation 5.2 the dissipated power that caused the temperature increase.

$$P_d = \frac{C \cdot \Delta T}{t},$$ (5.2)

where P_d represents the dissipated power (in W), C the thermal capacity of fat tissue (in J/°C), ΔT the variation of temperature (in °C), and t the time (in seconds).

For characterization of MATLAB's Penne's bioheat function, the values listed in 5.4 of the required variables were considered. Once the power dissipated in each block of tissue is determined, the power density Q (in W/m^3) that we are depositing in the medium was calculated by the following equation:

$$Q = \frac{P_d}{V},$$ (5.3)

where V represents the tissue volume (in m^3). The obtained results for the different values of ΔT, P_d and Q to a certain voltage and for a time t of 1200 s are presented in table 5.5.

Table 5.4: Tissues Properties defined for MATLAB simulations.

Property	Value	Unit
Fat specific heat	2348	J/kg.°C
Fat density	911	Kg/m^3
Fat thermal conductivity	0.171	W/m.°C
Fat blood perfusion	0.00008	1/s
Blood specific heat	3770	J/kg.°C
Blood density	1060	Kg/m^3
Arterial Temperature	37	°C

Table 5.5: Values of power density Q and P_d for the different voltages.

Voltage (V)	ΔT (°C)	P_d (W)	Q (W/m^3)
0.01	3.87e-3	8.623e-7	6.898
0.1	0.39	8.689e-5	695.184
0.5	9.68	2.157e-3	17254.826

After running both simulations, it was possible to obtain the different values as shown in tables 5.6, 5.7 and 5.8. In addition, simulations in MATLAB were performed in MATLAB for

both cases, counting on the blood perfusion contribution ($P > 0$) and not considering the blood perfusion influence ($P = 0$).

Table 5.6: Final temperature (in °C) reached at each block of fat tissue, represented as 1, 2, 3 and 4 for both simulations, at 9.583e-11 W.

	1	**2**	**3**	**4**
ADS	37.0039	37.0039	37.0039	37.0039
MATLAB ($P = 0$)	37.0039	37.0039	37.0039	37.0039
MATLAB ($P > 0$)	37.0035	37.0035	37.0035	37.0035

Table 5.7: Final temperature (in °C) reached at each block of fat tissue, represented as 1, 2, 3 and 4 for both simulations, for 9.853e-9 W.

	1	**2**	**3**	**4**
ADS	37.39	37.39	37.39	37.39
MATLAB ($P = 0$)	37.39	37.39	37.39	37.39
MATLAB ($P > 0$)	37.35	37.35	37.35	37.35

Table 5.8: Final temperature (in °C) reached at each block of fat tissue, represented as 1, 2, 3 and 4 for both simulations, at 2.396e-7 W.

	1	**2**	**3**	**4**
ADS	46.68	46.68	46.68	46.68
MATLAB ($P = 0$)	46.68	46.68	46.68	46.68
MATLAB ($P > 0$)	45.86	45.86	45.86	45.86

From the obtained results of both simulations, it is possible to observe that the final temperatures are the same, concerning $P = 0$ in MATLAB simulation. Furthermore, from the analysis of temperature variation for the simulations performed in MATLAB counting with blood perfusion or not, it is possible to verify that tissue's vascularization has influence on the final temperature reached, being smaller when $P > 0$.

5.2   Tridimensional Equivalent Electrical Model of Biological Tissues

Regarding to the 3-D equivalent electrical model of biological tissues, were performed simulations were performed within the ADS Software to understand how the model behaves. The voltage was set to 0.01 V corresponding to an incident power of 8.818e-8 W, at 13.56 MHz. In this sense, for each tissue block that constitutes the different layers, the current I (in *A*) and the dissipated power Pd (in *W*) were measured. In addition, also the voltage V was measured, and it is verified that it is constant for each layer of tissue. The obtained results for the different layers are presented in the tables 5.9, 5.10 and 5.11.

Table 5.9: Current and dissipated power measured in ADS in the different tissue blocks of skin layers.

Tissue Block	I (A)	P_d (W)
_59	3.878e-6	3.622e-10
_64	3.648e-6	3.054e-10
_67	3.878e-6	3.622e-10
_60	3.648e-6	3.054e-10
_63	5.169e-6	1.687e-9
_66	3.648e-6	3.054e-10
_61	3.878e-6	3.622e-10
_62	3.648e-6	3.054e-10
_65	3.878e-6	3.622e-10

Table 5.10: Current and dissipated power measured in ADS for the different tissue blocks fat layer, where block _30 represents a tumor.

Tissue Block	I (A)	P_d (W)
_74	1.270e-6	3.472e-10
_75	1.230e-6	3.282e-10
_76	1.270e-6	3.472e-10
_72	1.230e-6	3.282e-10
_30	8.211e-6	7.368e-10
_69	1.230e-6	3.282e-10
_73	1.270e-6	3.472e-10
_71	1.230e-6	3.282e-10
_70	1.270e-6	3.472e-10

Table 5.11: Current and dissipated power measured in ADS for the different tissue blocks gland layer, where block _81 represents a tumor.

Tissue Block	I (A)	P_d (W)
_79	7.560e-7	1.631e-11
_31	7.871e-7	3.472e-11
_83	7.560e-7	1.631e-11
_78	7.871e-7	3.472e-11
_81	8.500e-6	4.581e-10
_84	7.871e-7	3.472e-11
_77	7.560e-7	1.631e-11
_80	3.648e-6	3.472e-11
_85	7.560e-7	1.631e-11

From the analysis of these results, it is possible to observe that in skin layer for larger values of current I, dissipated power P_d is higher. Since the voltage V is constant, and according to Ohm's law $V = R \cdot I$ for higher values of I, had to correspond smaller values of resistance R. Once V is constant, and the power is given by $P = V^2/R$, for smaller values of R (higher I) the dissipated power will be higher. Similarly, for fat layer, it is possible to verify that for a constant V for the

elements where current is larger (smaller R) the dissipated power is higher. The same is verified in the gland layer.

Moreover, it is possible to see that between skin layer and fat layer the P_d is larger for skin than fat tissue. Once the voltage V is practically constant, it is possible to observe that current is much smaller in fat layer than in skin. Therefore, for smaller I, the values of resistance are higher and since $P = V^2/R$, P_d is smaller in fat layer. The same is possible to verify between fat and gland, and, in turn, between skin and gland layer.

Regarding to tumour tissue, it is possible to observe that current is higher when compared to the other elements in each layer and, in turn, the power dissipated is higher, as it was expected since tumour tissue shows better conductivity than the others. One possible reason that can influence the differences of P_d between tumours is the contribution of the surrounding tissues. Since fat is more resistive, i.e., higher values of R, current is smaller in fat than in gland. Once between tumour tissue current is practically constant, once power is given by $P = R \cdot I^2$ then, for high values of R, P_d for tumour surrounded by fat layer is higher than that compared to gland.

To understand how this model is sensible to the variations of surrounding tissues, another simulation considering a different location of tumour was performed. The same voltage value and frequency were set but the tumour in gland was moved for fat layer. After running the simulations, it is possible to obtain these different values as shown in the tables 5.12, 5.13 and 5.14.

Table 5.12: Current and dissipated power measured in ADS for the different blocks of tissue that constitute the skin layer.

Tissue Block	I (A)	P_d (W)
_59	4.096e-6	3.861e-10
_64	5.497e-6	1.198e-9
_67	4.096e-6	3.861e-10
_60	3.449e-6	2.686e-10
_63	4.769e-6	1.148e-9
_66	3.648e-6	2.686e-10
_61	3.610e-6	3.142e-10
_62	3.359e-6	2.582e-10
_65	3.610e-6	3.142e-10

After comparing both results, it is possible to verify that, despite the different values for I and P_d according to the location of tumour, the model follows the same behaviour, i.e., once the voltage is constant between the different layers, where the current is higher, power dissipated is higher once that for higher currents, lower resistance, and since for a constant V, power is given by $P = V^2/R$ it is possible to see an agreement in results.

5.3 Thermal Modelling of Heating of Biological Tissues

Considering the thermal model, relating the values of power dissipated in each block of tissue with the temperature, would be expectable that for higher values of dissipated power the temperature

Table 5.13: Current and dissipated power measured in ADS for the different blocks of tissue that constitute the fat layer, where block _75 and _30 represent a tumor.

Tissue Block	I (A)	P_d (W)
_74	1.012e-6	2.138e-10
_75	5.952e-6	3.597e-10
_76	1.012e-6	2.138e-10
_72	1.010e-6	2.168e-10
_30	6.431e-6	4.289e-10
_69	1.010e-6	2.168e-10
_73	1.075e-6	2.449e-10
_71	1.025e-6	2.252e-10
_70	1.075e-6	2.449e-10

Table 5.14: Current and dissipated power measured in ADS for the different blocks of tissue that constitute the gland layer.

Tissue Block	I (A)	P_d (W)
_79	4.998e-7	3.200e-11
_31	5.713e-6	2.359e-10
_83	4.998e-7	3.200e-11
_78	5.984e-7	3.374e-11
_81	6.319e-6	2.950e-10
_84	5.984e-7	3.374e-11
_77	5.731e-7	1.903e-11
_80	6.201e-7	3.944e-11
_85	5.731e-7	1.903e-11

reached in each block was higher. Regarding to ADS simulations, first, the model with the tumour located in both fat and gland tissue was simulated. The incident power considered was 8.818e-8 W, during 1200 s. The obtained results for the different tissue layers are listed in the table 5.15.

Table 5.15: Temperature measured in ADS for the different blocks of tissue for skin, fat and gland layer, where block _30 and _81 represents tumor tissue.

Tissue Block (Skin Layer)	Temp. (°C)	Tissue Block (Fat Layer)	Temp. (°C)	Tissue Block (Gland Layer)	Temp. (°C)
_59	37.18	_74	37.17	_79	37.01
_64	37.15	_75	37.16	_31	37.02
_67	37.18	_76	37.17	_83	37.01
_60	37.15	_72	37.16	_78	37.02
_63	37.84	_30	37.37	_81	37.23
_66	37.15	_63	37.16	_84	37.02
_61	37.18	_73	37.17	_77	37.01
_62	37.15	_71	37.16	_80	37.02
_65	37.18	_70	37.17	_85	37.01

It can be seen that the temperature varies according to what is predicted by the electrical model

analysis, i.e., for higher values of power dissipated, higher is the temperatures are also reached in the tissue.

To study the influence of incident power and the dissipated power in tissues heating, some simulations for different voltages were performed in ADS to see how the temperature varies in tissues. The results obtained for simulations at 0.02 V and 0.03 V with an incident power of 3.5272e-7 W and 7.9362e-7 W, respectively, during 1200 s are presented in in the tables 5.16 and 5.17.

Table 5.16: Temperature measured in ADS for the different blocks of tissue for skin, fat and gland layer, where block _30 and _81 represents tumor tissue, for 3.5272e-7 W.

Tissue Block (Skin Layer)	Temp. (°C)	Tissue Block (Fat Layer)	Temp. (°C)	Tissue Block (Gland Layer)	Temp. (°C)
_59	37.72	_74	37.69	_79	37.03
_64	37.61	_75	37.66	_31	37.07
_67	37.72	_76	37.69	_83	37.03
_60	37.61	_72	37.66	_78	37.07
_63	40.36	_30	38.47	_81	37.91
_66	37.61	_63	37.66	_84	37.07
_61	37.72	_73	37.69	_77	37.03
_62	37.61	_71	37.66	_80	37.07
_65	37.72	_70	37.69	_85	37.03

Table 5.17: Temperature measured in ADS for the different blocks of tissue for skin, fat and gland layer, where block _30 and _81 represents tumor tissue, for 7.9362e-7 W.

Tissue Block (Skin Layer)	Temp. (°C)	Tissue Block (Fat Layer)	Temp. (°C)	Tissue Block (Gland Layer)	Temp. (°C)
_59	38.63	_74	38.56	_79	37.07
_64	38.38	_75	38.48	_31	37.16
_67	38.63	_76	38.56	_83	37.07
_60	38.38	_72	38.48	_78	37.16
_63	44.55	_30	40.31	_81	39.05
_66	38.38	_63	38.48	_84	37.16
_61	38.63	_73	38.56	_77	37.07
_62	38.38	_71	38.48	_80	37.16
_65	38.63	_70	38.56	_85	37.07

By the analysis of both results, it is possible to verify that with the increasing of V, higher temperature is reached. However, as we increase the voltage, the temperature of block _63, in skin, heats too much when compared to the surrounding tissues. One possible reason for this phenom can be explained by the fact that it is connected to the tumour, and since the tumour has higher conductivity than skin, once the voltage is practically constant, when compared to fat, current is superior in skin and because of that R is smaller for skin leading to higher values of power dissipated tumour associated to skin and, in turn, greater increase of temperature.

One possible way to counteract the undesirable overheating of the element _63 is to decrease the incident power and increase the time of heating. However, from the simulations performed it was verified that by increasing the time to 2700 s (45 minutes) the results obtained for 3.5272e-7 W were the same to those obtained for 7.9362e-7 W during 1200 s.

The same study was performed for the second model, considering tumour tissue location only in fat tissue. The obtained results of temperature of each tissue layer, for the different values of voltage during 1200 s are listed in the tables 5.18, 5.19 and 5.20.

Table 5.18: Temperature measured in ADS for the different blocks of tissue for skin, fat and gland layer, where block _81 and _93 represents tumor tissue, for 8.984e-8 W.

Tissue Block (Skin Layer)	Temp. (°C)	Tissue Block (Fat Layer)	Temp. (°C)	Tissue Block (Gland Layer)	Temp. (°C)
_59	37.19	_74	37.11	_79	37.02
_64	37.60	_81	37.18	_94	37.15
_67	37.19	_76	37.11	_83	37.02
_60	37.13	_72	37.11	_78	37.02
_63	37.57	_93	37.21	_89	37.12
_66	37.13	_69	37.11	_84	37.02
_61	37.16	_73	37.12	_77	37.01
_62	37.13	_71	37.11	_80	37.02
_65	37.16	_70	37.12	_85	37.01

Table 5.19: Temperature measured in ADS for the different blocks of tissue for skin, fat and gland layer, where block _81 and _93 represents tumour tissue, for 3.5936e-7 W.

Tissue Block (Skin Layer)	Temp. (°C)	Tissue Block (Fat Layer)	Temp. (°C)	Tissue Block (Gland Layer)	Temp. (°C)
_59	37.77	_74	37.43	_79	37.06
_64	39.39	_81	37.72	_94	37.59
_67	37.77	_76	37.43	_83	37.06
_60	37.54	_72	37.43	_78	37.07
_63	39.29	_93	37.86	_89	39.47
_66	37.54	_69	37.43	_84	37.07
_61	37.63	_73	37.49	_77	37.04
_62	37.52	_71	37.45	_80	37.08
_65	37.63	_70	37.49	_85	37.04

From the various simulations, it is possible to observe that, as it was expected, for the different tumour location, the final tissues' temperatures will vary according to the power dissipated associated to each block of tissue. Despite the differences, it can be observed that the model behaves similarly, i.e., for higher values of power dissipated, in the electrical model, the temperature measured, in thermal model, is also higher.

However, the final temperature reached in tumour tissues it is not enough for ablation. In this sense, other simulations were performed considering the same values of voltage but during 2700

Table 5.20: Temperature measured in ADS for the different blocks of tissue for skin, fat and gland layer, where block _81 and _93 represents tumor tissue, for 8.0856e-7 W.

Tissue Block (Skin Layer)	Temp. (°C)	Tissue Block (Fat Layer)	Temp. (°C)	Tissue Block (Gland Layer)	Temp. (°C)
_59	38.74	_74	37.96	_79	37.15
_64	42.37	_81	38.62	_94	38.32
_67	38.74	_76	37.96	_83	37.15
_60	38.21	_72	37.98	_78	37.15
_63	42.14	_93	38.93	_89	38.06
_66	38.21	_69	37.98	_84	37.15
_61	38.41	_73	38.10	_77	37.09
_62	38.17	_71	38.01	_80	37.18
_65	38.41	_70	38.10	_85	37.09

s (45 minutes). From the obtained results, it was possible to verify that for for 8.0856e-7 W the temperature reached in the tissues is very high, which can lead to undesirable normal tissue lesion, and for 3.5936e-7 W it obtained the same final temperature than for 7.9362e-7 W at a heating time of 1200 s.

5.4   Conclusions

From this chapter, it is important to note that the simulation of EM propagation within tissues as well as tissues heating can be influenced by several factors.

Regarding to the linear equivalent model validation, it is possible to observe that a good approximation of what is expectable from theoretical curve was accomplished. In addition, when the model was adapted including also the modelling of heat transfer within tissues, to study the variation of temperature along 1-D, it is possible to verify that also a good approximation of what was expectable from the Penne's bioheat equation was accomplished. However, from the obtained results when the blood perfusion is considered, the temperature measured in MATLAB is lower than the one obtained in ADS. Despite in this model were considered the values of k_{eff}, as previously explained, lead to the conclusion that this consideration is not enough to produce a more accurate value of the influence of blood perfusion in tissues heating.

With respect to results of 3-D equivalent electrical model of biological tissues, it is possible to realize that both simulations provide similarly results. Despite the differences found for the influence of different contribution of the surrounding tissues, it is verified that the power dissipated is higher for higher current values or, in other words, for smaller resistance values, dissipated power is higher. In addition, when the modelling of tissues heating is including by means of thermal model, it is possible to observe that for higher values of dissipated power a greater final temperature is reached.

Chapter 6

Conclusions and Future Work

Thermal ablation can be defined as the direct application of chemical or thermal therapies to a tissue to cause its eradication or substantial destruction. Hence, hyperthermia ablation refers to complete (systemic) or partial (local/regional) destruction of a tissue by application of heat or elevation of temperature. Concerning the heating methods used for hyperthermia, there are two main processes for ablation: systemic and local. These constitute two large groups of alternatives treatments, which are involved in different physiological actions and support different reaction mechanisms. Thus, there is a wide-range of different heat generation/application techniques which can be used for heating the tissues. With respect to hyperthermia ablation based on electromagnetic waves for the treatment of tumors, it is possible to realize that, first, the techniques can be classified according to the frequency range, in ultrasound, radiofrequencies or microwaves. On the other hand, it is possible to realize that the purpose of these techniques is to destroy all the cancerous tissue as well as a significant margin of normal tissue that surrounds it, to prevent a possible recurrence of the tumor. Concerning to these three methods, the proper choice of the ablation method depends not only on the patient's conditions but also on the size and location of the tumor. For tumors up to three centimeters in diameter, any of the techniques can achieve good therapeutic effects, however, radiofrequency ablation is the most appropriate since the electrodes can be adjusted to protect adjacent organs. For tumors with a diameter greater than five centimeters, the microwave ablation technique is the most adequate approach due to its ability to reach higher intratumorally temperatures and, consequently, higher volumes of ablation.

Secondly, it is possible to realize that for understanding the phenomenon of tissue heating by electromagnetic radiation, it is important to have a notion that the human organism itself has the ability to maintain its body temperature constant and because of that, when undergoing variations of temperature by the application of external energy sources, the thermoregulation mechanisms will be triggered which will counteract this variation, which may affect the whole treatment process of tumor ablation by hyperthermia.

In addition, it is necessary to consider the different mechanisms of heat dissipation that can occur during the propagation of radiation along the tissues, since these are factors that not only determine the final temperature that can be reached but also the exposure time to which the pa-

tient can or must be exposed. These factors can be combined in a single equation, called Penne's bio-heating equation, which allows the resulting temperature to be obtained after exposure to electromagnetic radiation. To understand this phenomenon, most of the studies are governed by computational simulations based on advanced numerical methods, such as the finite element method (FEM) and finite difference method (FDTD). For this, there are several simulation tools that allow the construction of models, resolution by numerical methods referred to, simulation and post-processing of results, such as COMSOL Multiphysics, Sim4life and Ansys. However, although these methods are a very efficient, fast and accurate tool that provides a means of calculation in the three-dimensional domain of electromagnetic fields and temperature, they do not allow the realization in a single environment of simulations that also include the electronic circuits of the generating systems of electromagnetic radiation.

To bring the electromagnetic propagation and the heating of tissues to the domain of the electrical simulation, to obtain a unique environment of simulation of the entire process, an equivalent electrical model was developed that allows to simulate the propagation and the effect of the EM radiation interference in biological tissues for one spatial dimension. With the optimization of the linear model to three-dimensions, it is intended not only to obtain a more realistic view of the process to better understand how, effectively, the propagation of radiation occurs but also to have a better perception of how the distribution of heating occurs, along the tissues.

Regarding to the 1-D linear equivalent electrical model, it works according to what was theoretically expected. In addition, it is possible to verify that the model is sensible enough to measure the variations in dissipated power when the contribution of the body was considered. Moreover, comparing both results obtained from the ADS simulations and MATLAB, a satisfactory result of temperature variation in tissues is obtained. With respect to the model optimization to three dimensions, from the simulations results, it is possible to observe that, when different locations of tumor and, in turn, different contributions of the surrounding tissues are considered, the values of temperature measured in the thermal model vary according to what was expected. Thus, it is possible to verify that this model is also sensible enough to measure the variations of power dissipated in the different elements that constitute each tissue layer, which in turn has led to a reasonable result obtained in the field of temperatures.

In this sense, regarding to the goals of this dissertation, it is possible to conclude that the developed model at 1-D and its optimization for 3-D gives a good approximation of what happens in tissues not only for EM radiation propagation but also for heating of tissues.

6.1   Future Work

With aim of improving the obtained results, it is possible to consider some different approaches of work.

Regarding to the accuracy of temperature results, it should be though of how the dissipation through bloodstream can be included in this model.

Furthermore, through the validation simulations it was possible to verify that greater values of power dissipated are obtained for 2 GHz. In this sense, it would be interesting to perform a sweep of frequencies to realize what is the optimum frequency value to obtain a higher power dissipation, and consequently a higher temperature reached in the tissues.

In addition, the realization of experimental trials, reproducing the same conditions of the model, it would be an important step for validation of the model when compared to a realistic scenario of hyperthermia treatment. Besides, it would be interesting to perform the same experimental trials but also considering the antenna emitting on the desired point to be heated.

Appendix A

Matlab Code

```
function [T, T_change, kgrid, dx] =
    bioheatExact(T0, S, material, dx, t)
% BIOHEATEXACT Compute exact solution to Pennes' bioheat
% equation in homogeneous media.
%
% DESCRIPTION:
%     bioheatExact calculates the exact solution to Pennes'
%     bioheat equation in a homogeneous medium on a uniform
%     Cartesian grid using a Fourier-based Green's function
%     solution assuming a periodic boundary condition [1].
%     The function supports inputs in 1D, 2D, and 3D.
%     The exact equation solved is given by
%
%         dT/dt = D * d^2T/dx^2 - P * (T - Ta) + S
%
%     where the coefficients are defined below. Pennes' bioheat
%     equation is often given in the alternative form
%
%         P0 * C0 * dT/dt =
%            Kt * d^2T/dx^2 - Pb * Wb * Cb * (T - Ta) + Q
%
%         T:  temperature                    [degC]
%         C0: tissue specific heat capacity   [J/(kg.K)]
%         P0: tissue density                  [kg/m^3]
%         Kt: tissue thermal conductivity     [W/(m.K)]
%         Pb: blood density                   [kg/m^3]
%         Wb: blood perfusion rate            [1/s]
%         Ta: blood arterial temperature      [degC]
```

```
%             Cb:  blood specific heat capacity     [J/(kg.K)]
%             Q:   volume rate of heat deposition   [W/m^3]
%
%     In this case, the function inputs are calculated by
%
%             D = Kt / (P0 * C0);
%             P = Pb * Wb * Cb / (P0 * C0);
%             S = Q / (P0 * C0);
%
%     If the perfusion coefficient P is set to zero,
%     bioheatExact calculates the exact solution to the
%     heat equation in a homogeneous medium.
%
%     [1] Gao, B., Langer, S., & Corry, P. M. (1995).
%     Application of the time-dependent Green's function and
%     Fourier transforms to the solution of the bioheat equation
%     International Journal of Hyperthermia, 11(2), 267-285.
%
% USAGE:
%     T = bioheatExact(T0, S, material, dx, t)
%     T = bioheatExact(T0, S, [D, P, Ta], dx, t)
%
% INPUTS:
%     T0        - matrix of the initial temperature distribution
%                 at each grid point [degC]
%     S         - matrix of the heat source at each grid
%                 point [K/s]
%     material  - material coefficients given as a three element
%                 vector
%                 in the form: material = [D, P, Ta], where
%
%                     D:  diffusion coefficient [m^2/s]
%                     P:  perfusion coefficient [1/s]
%                     Ta: arterial temperature  [degC]
%
%     dx        - grid point spacing [m]
%     t         - time at which to calculate the temperature
%                 field [s]
%
% OUTPUTS:
```

```
%       T               − temperature field at time t [degC]
%
% ABOUT:
%       author      − Bradley Treeby and Teedah Saratoon
%       date        − 18th August 2015
%       last update − 11th June 2017
%
% This function is part of the k−Wave Toolbox
% (http://www.k−wave.org)
% Copyright (C) 2015−2017 Bradley Treeby and Teedah Saratoon
%
% See also kWaveDiffusion

% This file is part of k−Wave. k−Wave is free software: you can
% redistribute it and/or modify it under the terms of the GNU
% Lesser General Public License as published by the Free
% Software Foundation, either version 3 of the License, or
% (at your option) any later version.
% k−Wave is distributed in the hope that it will be useful,
% but WITHOUT ANY WARRANTY; without even the implied warranty of
% MERCHANTABILITY or FITNESS FOR A PARTICULAR PURPOSE.   See the
% GNU Lesser General Public License for more details.
%
% You should have received a copy of the
% GNU Lesser General Public
% License along with k−Wave. If not,
% see <http://www.gnu.org/licenses/>.

% check that T0 is a matrix
if numel(T0) == 1
    error('T0 must be defined as a matrix.');
end

% if S is not 0, check that S and T0 are the same size
if ~((numel(S) == 1) && (S == 0)) && ~all(size(S) == size(T0))
    error('T0 and S must be the same size.')
end

% extract material properties
D  = material(1);   % difusion coefficient
```

```matlab
P  = material(2);    % perfusion coefficient
Ta = material(3);    % blood arterial temperature

% check the medium properties are homogeneous
if numel(P) > 1 || numel(D) > 1 || numel(Ta) > 1
    error('Medium properties must be homogeneous.');
end

% create the set of wavenumbers
kgrid =
    kWaveGrid(size(T0, 1), dx,
              size(T0, 2), dx,
              size(T0, 3), dx);

% define Green's function propagators
T0_propagator =
    exp(-(D .* ifftshift(kgrid.k).^2 + P) .* t);
Q_propagator =
    (1 - T0_propagator) ./ (D .* ifftshift(kgrid.k).^2 + P);

% replace Q propagator with limits for k == 0
%     if P == 0, the limit is t
%     if P ~= 0, the limit is (1 - exp(-P*t))/P
if (numel(P) == 1) && (P == 0)
    Q_propagator(isnan(Q_propagator)) = t;
else
    Q_propagator(isnan(Q_propagator)) = (1 - exp(-P .* t)) ./ P;
end

% calculate exact Green's function solution (Eq. 12 [1])
if (numel(S) == 1) && (S == 0)
    T_change = real(ifftn( T0_propagator .* fftn(T0 - Ta) ));
else
    T_change =
        real(ifftn( T0_propagator .* fftn(T0 - Ta) +
                    Q_propagator .* fftn(S) ));
end
T = T_change + Ta;


Kt = 0.171;
```

```matlab
C0 = 2348;
P0 = 911;
Q = 1553.6473;
T0 = [37;  37;  37;  37];
S = [Q/(P0*C0);  Q/(P0*C0);  Q/(P0*C0);  Q/(P0*C0)];
D = Kt/(P0*C0);
P = 0;
% Pb = 1060;
% Wb = 0.00008;
% Cb = 3770;
% P = Pb * Wb * Cb / (P0 * C0);
Ta = 37;
dx = 0.005;
t = 1200;
[T, T_change, kgrid, dx] = bioheatExact(T0, S, [D,P,Ta], dx, t);
```

References

[1] European Commission. Electromagnetic fields - update 2009. Available: http://ec.europa.eu/health/scientific_committees/opinions_layman/en/electromagnetic-fields/electromagnetic-fields-greenfacts-level2.pdf Access on: 15/02/2018.

[2] Depts. Washington. Eletromagnetic radiation. Available: https://depts.washington.edu/cmditr/modules/lum/electromagnetic_radiation.html Access on: 15/02/2018.

[3] A. C. Metaxas and R. J. Meredith. *Industrial Microwave Heating*, volume 1 of *IEE Power Engineering Series 4*. Peter Peregrinus Ltd., London, UK, 1983.

[4] S. Pattanaik. Biolofical effects of rf/mw radiations on human. *Arch. Appl. Sci. Res.*, 4(1):381–387, 2012.

[5] V. F. M. Vieira. Effect of electromagnetic fields induced by mobile devices in human brain. Master's thesis, Departamento de Engenharia Eletrónica, FEUP, Porto, Portugal, 2017.

[6] T. H. Wendell. *Electromagnetic Radiation*. Wiley-VCH Verlag GmbH and Co. KGaA, Weinheim, Germany, 3 edition, 2009.

[7] R. W. Y. Habash. Bioeffects and therapeutic applications of electromagnetic energy. *Arch. Appl. Sci. Res.*, 2008.

[8] M. Francisco and J. Cepeda. *High Temperature Hyperthermia in Breast Cancer Treatment*. May 15 2013. Available: https://www.intechopen.com/books/hyperthermia/high-temperature-hyperthermia-in-breast-cancer-treatment Access on: 9/10/2017.

[9] J. P. Mcgahan and G. D. Dodd III. Radiofrequency ablation of the liver: Current status. *American Journal of Roentgenology*, (176):3–16, January 2001.

[10] D. E. Dupuy C. J. Simon and W. William. Microwave ablation: Principles and applications. *RadioGraphics*, (25):69–83, 2005.

[11] C. Lafon F. Prat and D. Cathignol. A high-intensity us probe designed for intraductal tumor destruction: experimental results. *Gastrointestinal Endoscopy*, (50):388–392, 1999.

[12] Freescale Semiconductor Inc. Thermal analysis of semiconductor systems, 2008.

[13] H. Bengtson. Combined thermal conduction and convection heat transfer calculations. 2011. Available: https://www.brighthubengineering.com/hvac/62074-combined-thermal-conduction-and-convection-heat-transfer-calculations/#disqus_thread Access on: 4/05/2018.

[14] Webster's New World College Dictionary. Cube, 1998. Available: http://websters.yourdictionary.com/cube Access on: 17/08/2018.

[15] B. Seitzand and I. Jung. Painted sides of a cube, 1998. Available: http://jwilson.coe.uga.edu/EMT668/EMT668.Student.Folders/SeitzBrian/EMT669/painted.cube/painted.html Access on: 17/08/2018.

[16] R. Rossi D. Andreuccetti and C. Petrucci. An internet resource for the calculation of the dielectric properties of body tissues in the frequency range 10 hz – 100 ghz. *IFAC-CNR*, 1997. Based on data published by C. Gabriel et al. in 1996, Available:http://niremf.ifac.cnr.it/tissprop/htmlclie/htmlclie.php Access on: 9/03/2018.

[17] C. L. Brace. Radiofrequency and microwave ablation of the liver, lung, kidney, and bone: What are the differences? *YMDR*, 38(3):135–143, 2009.

[18] A. V. Hernández L. L. Salas E. Ávila-Navarro M. Francisco, J. Cepeda and E. A. Navarro. Coaxial slot antenna design for microwave hyperthermia using finite- difference time-domain and finite element method. *The Open Nanomedicine Journal*, (3):2–9, 2011.

[19] V. Muralidharan M. Nikfarjam and C. Christophi. Mechanisms of focal heat destruction of liver tumors. *Journal of Surgical Research*, 223(127):208–223, 2005.

[20] C. Brace. Thermal tumor ablation in clinical use. *IEEE pulse*, 5(2):28–38, 2011.

[21] S. Labonté. Numerical model for radio-frequency ablation of the endocardium and its experimental validation. *IEEE Transactions on Biomedical Engineering*, 41(2), 1994.

[22] Site by Comsol Inc. Understand, predict, and optimize engineering designs with the comsol multiphysics software, 2018. Available: https://www.comsol.com/comsol-multiphysics Access on: 20/10/2017.

[23] Site by Ansys Inc. Products, 2018. Available: https://www.ansys.com/products Access on: 20/10/2017.

[24] Site by ZMT Zurich Medtech AG. Understand, predict, and optimize engineering designs with the comsol multiphysics software, 2010-2017. Available: https://www.comsol.com/comsol-multiphysics Access on: 20/10/2017.

[25] Z. Psenakova and V. Psenák. Eletromagnetic heating of human tissue. volume 2. YBERC 2005, ACTA MECHANICA SLOVACA, 1 2005.

[26] M. J. Rivera, Juan A. Lopez Molina, M. Trujillo, Vicente Romero-García, and Enrique J. Berjano. Analytical validation of comsol multiphysics for theoretical models of radiofrequency ablation including the hyperbolic bioheat transfer equation. *2010 Annual International Conference of the IEEE Engineering in Medicine and Biology*, pages 3214–3217, 2010.

[27] E. M. Leidholot J. T. Bushberg, J. A. Seibert and J. M. Boone. *The Essential Physics of Medical Imaging*. Lippincott Williams and Wilkins, Philadelphia, USA, 3 edition, 2012.

[28] K. Boyle Y. Huang. *Antennas from Theory to Practice*. John Wiley and Sons, Chichester, UK, 1 edition, 2008.

[29] D. K. Cheng. *Field and Wave Electromagnetics*. Addison-Wesley Publishing Company, USA, 1 edition, 1983.

[30] S. Gomes. Therapeutic applications of electromagnetic radiation. Master's thesis, Departamento de Engenharia Eletrónica, FEUP, Porto, Portugal, 2016.

[31] Eric Chow, Chin Chin-Lung, Yuehui Ouyang, Arthur Chlebowski, Pedro Irazoqui, and William J. Chappell. Chapter 9: Wireless powering and propagation of radio frequencies through tissue. pages 301–336, July 2012. Available: `https://depts.washington.edu/cmditr/modules/lum/electromagnetic_radiation.html` Access on: 27/11/2017.

[32] D. Razansky H. Estrada, J. Rebling. Prediction and near field observation of skull-guided acoustic waves. *Phys. Med. Biol.*, 62:4728–4740, 2017.

[33] World Heath Organization. Establishing a dialogue on risks from electromagnetic fields. 2002. Available: `http://www.who.int/peh-emf/publications/en/EMF_Risk_ALL.pdf` Access on: 15/02/2018.

[34] Norwegian Institute of Public Health. Low-level radiofrequency electromagnetic fields - an assesment of health risks and evaluation of regulatory practice. 2002. Available: `https://www.fhi.no/globalassets/dokumenterfiler/rapporter/2012/low-level-radiofrequency-electromagnetic-fields--an-assessment-of-health-risks-and-evaluation-of-regulatory-practice.-niph-report-20123.pdf` Access on: 15/02/2018.

[35] L. S. Erdreich and B. J. Klauenberg. Radio frequency radiation exposure standards: Considerations for harmonization. *Health Phys*, 80(5):430–439, 2001.

[36] J. A. Nyenhuis M. Phillips F. G. Shellock J. González-Martinez K. B. Baker, J. A. Tkach and A. R. Rezai. Evaluation of specific absorption rate as a dosimeter of mri-related implant heating. *J. Magn. Reson. Imaging*, 20:315–320, 2004.

[37] I. Cosic E. Pirogova, V. Vojizavlzevic. Biological effects of electromagnetic radiation. *Biomedical Engineering*, 2009.

[38] D. Coluccia et al. First noninvasive thermal ablation of a brain tumor with mr-guided focused ultrasound. *Journal of Therapeutic Ultrasound*, 2(17):1–7, 2014.

[39] B. Postic B. Marmor and M. Hahn. Treatment of superficial human neoplasms by local hyperthermia induced by ultrasound. *Cancer*, 43(1):188–197, 1979.

[40] S. Th M. Marberger S. Crouzet E. R. Cordeiro, X. Cathelineau and J. J. M. C. H. De Rosette. Review article: High-intensity ultrasound (hifu) for definitive treatment of prostate cancer. *BJU International*, 110(9):1228–42, 2012.

[41] Site by INSIGHTEC Ltd. Insightec for oncology, 2018. Available: `https://www.insightec.com/clinical/oncology` Access on: 7/03/2018.

[42] G. T. Haar and C. Coussios. High intensity focused ultrasound: Physical principles and devices. *International Journal of Hyperthermia*, 23:89–104, March 2007.

[43] C. VanPutte J. Regan and A. Russo. *Seeley's Essentialis of Anatomy Physiology*. McGraw-Hill Education, New York, USA, 2016.

[44] M. A. Khanday and K. Nazir. Mathematical and numerical analysis of thermal distribution in cancerous tissues under the local heat therapy. *International Journal of Biomathematics*, 10(7):1–10, 2017.

[45] H. S. Kou T. C. Shih and W. L. Lin. Effect of effective conductivity on thermal dose distributions of living tissue with directional blood flow during thermal therapy. *Int. Comm. Heat Mass Transfer*, 29(1):115–126, 2002.

[46] R. W. Lau S. Gabriel and C. Gabriel. The dielectric properties of tissues: III. parametric models for the dielectric spectrum of tissue. *Phys. Med. Biol.*, 41:2271–2293, 1996.

[47] S. Gabriel C. Gabriel and E. Corthout. The dielectric properties of tissues: I. literature survey. *Phys. Med. Biol.*, 41:2231–2249, 1996.

[48] E. R. War L. Sha and B. Stroy. A review of dielectric properties of normal and malignant breast tissue. *Proceedings IEEE SouthEast Con.*, 462, 2002.

[49] R. W. Lau S. Gabriel and C. Gabriel. The dielectric properties of tissues: II. measurements in the frequency range 10 hz to 20 ghz. *Phys. Med. Biol.*, 41:2251–2269, 1996.

[50] J. R. Barr A. J. Surowiec, S. S. Stuchy and A. Swarup. Dielectric properties of breast carcinoma and the surrounding tissues. *IEEE Transactions on Biomedical Engineering*, 35(4), 1988.

[51] M. D. Rafal W. T. Joines, R. L. Jirtle and D. J. Shaefer. Microwave power absorption differences betweem normal and malignant tissue. *Int. J. Radiation Oncology Biol. Phys.*, 6:681–687, 1980.

[52] C. Baumgartner E. Neufeld B. Lloyd M. C. Gosselin D. Payne A. Klingenbock P. A. Hasgall, E. Di Gennaro and N. Kuster. New materials for dielectric simulation of tissues. *Phys. Med. Biol.*, 36(12):1565–1571, 1991.

[53] H. F. Bowman. Heat transfer and thermal dosimetry. *Journal of Microwave Power*, 16(2):121–133, 1981.

[54] Gautherie M. Thermopathology of breast cancer: measurement and analysis of in vivo temperature and blood flow. *Annals of the New York Academy of Sciences*, 335:383–415, 1980.

[55] F. J. González. Thermal simulation of breast tumors. *Revista Mexicana de Física*, 53(4):323–326, 2007.

[56] C. Baumgartner E. Neufeld B. Lloyd M. C. Gosselin D. Payne A. Klingenbock P. A. Hasgall, E. Di Gennaro and N. Kuster. It'is database for thermal and electromagnetic parameters of biological tissues. Version 4.0, May 15 2018. DOI: 10.13099/VIP21000-04-0 Available: itis.swiss/database Access on: 27/04/2018.

[57] E. Y. K. Ng N. M. Sudharsan and S. L. Teh. Surface temperature distribution of a breast with and without tumour. *Computer Methods in Biomechanics and Biomedical Engineering*, 2(3):187–199, 1999.

[58] M. M. Osman and E. M. Afify. Thermal modelling of the normal woman's breast. *Journal of Biomechanical Engineering*, 106(2):123–30.

[59] A. S. Wright J. G. Webster D. Haemmerich, D. J. Schutt and D. M. Marhvi. Electrical conductivity measurement of excised human metastatic liver tumours before and after ablation. *Physiol. Meas.*, 30:459–466, 2009.

[60] B. R. Apstein R. G. Settle, K. M. Foster and J. L. Mullen. Nutritional assesment: Whole body impedance and body fluid compartments, nutrition and cancer. *Nutrition and Cancer*, 2(1):72–80, 1980.

[61] Zhang F. Marra, L and J. G. Lyng. Radiofrequency treatment of foods: Review of recent advances. *Journal of Food Engineering*, 91:491–508, 2009.

[62] Site by Keysight Technologies Inc. Custom modelling with symbolically-defined device, 2000-2018. Available: http://literature.cdn.keysight.com/litweb/pdf/ads2008/modbuild/ads2008/Custom_Modeling_with_Symbolically-Defined_Devices.html#CustomModelingwithSymbolically-DefinedDevices-1104314 Access on: 27/04/2018.

[63] A. Lakhssassi E. Kengne and R. Vaillancourt. Temperature distribution in living biological tissue simultaneously subjected to oscillatory surface and spatial heating: Analytical and numerical analysis. *International Mathematical Forum*, 7(48):2373–2393, 2012.